The Astrophysical Journal, 660:47–61, 2007 May 1

SPECTROSCOPY OF $z \sim 6$ *i*-DROPOUT GALAXIES: FREQUENCY OF Lyα EMISSION AND THE SIZES OF Lyα-EMITTING GALAXIES[1,2,3]

C. C. Dow-Hygelund,[4] B. P. Holden,[5] R. J. Bouwens,[5] G. D. Illingworth,[5] A. van der Wel,[6] M. Franx,[7] P. G. van Dokkum,[8] H. Ford,[6] P. Rosati,[9] D. Magee,[5] and A. Zirm[6]

Received 2006 February 25; accepted 2006 December 14

ABSTRACT

We report on deep spectroscopy, using LRIS on Keck I and FORS2 on the VLT, of a sample of 22 candidate $z \sim 6$ Lyman break galaxies (LBGs) selected by the $i_{775} - z_{850} > 1.3$ dropout criterion. Redshifts could be measured for eight objects. These redshifts are all in the range $z = 5.5$–6.1, confirming the efficiency of the $i_{775} - z_{850}$ color selection technique. Six of the confirmed galaxies show Lyα emission. Assuming that the 14 objects without redshifts are $z \sim 6$ LBGs that lack detectable Lyα emission lines, we infer that the fraction of Lyα-emitting LBGs with Lyα equivalent widths greater than 20 Å among $z \sim 6$ LBGs is ≈30%, similar to that found at $z \sim 3$. Every Lyα-emitting object in our sample is compact, with half-light radii $r_{\rm hl} \leq 0.14''$. Furthermore, all the Lyα-emitting objects in our sample are more compact than average relative to the observed size-magnitude relation of a large *i*-dropout sample (332 candidate $z \sim 6$ objects). We can reject the hypothesis that the Lyα-emitting population is a subset of the rest of the $z \sim 6$ LBG population at >97% confidence. We speculate that the small sizes of the Lyα-emitting LBGs are due to these objects being less massive than other LBGs at $z \sim 6$.

Subject headings: early universe — galaxies: evolution — galaxies: formation — galaxies: high-redshift — galaxies: starburst

1. INTRODUCTION

Distinguishing high-redshift galaxies from interlopers at lower redshifts can be a challenging process (Stern & Spinrad 1999). One particularly unique trait of high-redshift galaxies is the continuum break that they possess as a result of absorption by neutral hydrogen along the line of sight (Madau 1995; Dickinson 1999). Putting together this feature with the particularly blue colors of star-forming galaxies, we have a simple but efficient technique for selecting high-redshift star-forming galaxies (Steidel et al. 1995; Dickinson 1999). This technique has been extensively tested through spectroscopy on numerous Lyman break galaxies (LBGs) at $z \sim 2.5$–4.5 (Steidel et al. 1999) and on an increasing number of galaxies and quasars at $z \gtrsim 4$ (Weymann et al. 1998; Spinrad et al. 1998; Dey et al. 1998; Lehnert & Bremer 2003; Nagao et al. 2004; Fan et al. 2001; Bunker et al. 2003; Dickinson et al. 2004; Vanzella et al. 2006). In addition, there are now surveys that exploit narrowband excess from Lyα emission (see Taniguchi et al. 2003) to compile large (>20) samples of Lyα emitters (LAEs) at $z \approx 5.7$ (Rhoads et al. 2003; Hu et al. 2004; Shimasaku et al. 2005) and at $z \approx 6.6$ (Kashikawa et al. 2006; Stern et al. 2005).

Several groups utilizing these techniques have obtained statistically significant samples of galaxies at $z \sim 6$ (Rhoads & Malhotra 2001; Ajiki et al. 2003; Bouwens et al. 2003, 2004a, 2006; Stanway et al. 2003; Dickinson et al. 2004; Ajiki et al. 2006), as well as identifying candidate galaxies out to $z \sim 7$–8 (Hu et al. 2002; Kodaira et al. 2003; Bouwens et al. 2004b; Taniguchi et al. 2005; Stern et al. 2005; Rhoads et al. 2004; Kneib et al. 2004; Bouwens & Illingworth 2006; Iye et al. 2006). This has led to great progress in our understanding of the early universe, providing us with constraints on both the epoch of reionization (see Loeb & Barkana 2001; Fan et al. 2003; Malhotra & Rhoads 2004) and the evolution of the global star formation rate (SFR) density (Bouwens et al. 2003, 2004a, 2006; Hopkins 2004; Giavalisco et al. 2004). However, to ensure that these results are accurate, it is essential that we understand the nature of the galaxy populations being selected by these techniques and that we can quantify their relation to the underlying population of star-forming galaxies at $z \gtrsim 6$. This is paramount if we are to construct a self-consistent picture of the galaxy population from the different selection techniques. Issues that need to be addressed include (1) quantifying the distribution of Lyα equivalent widths for star-forming galaxies at $z \sim 6$, (2) determining the impact of these results on narrowband and broadband selections, and (3) using search results to construct a self-consistent picture of the galaxy population at $z \gtrsim 6$.

In this study, we use spectroscopy to study the nature of $z \sim 6$ i_{775}-dropouts identified by Bouwens et al. (2003, 2004a) in deep Advanced Camera for Surveys (ACS) imaging data. By contrasting the properties of our spectroscopic sample with similar selections at $z \sim 3$, we examine the evolution of the spectral properties of these sources with redshift. In addition, we pay particular attention to the implications of these results for future studies of high-redshift galaxies using either narrowband or broadband

[1] Based on observations taken with the W. M. Keck Observatory, which is operated as a scientific partnership among the California Institute of Technology, the University of California, and NASA.
[2] Based on observations made with the NASA / ESA *Hubble Space Telescope*, which is operated by the Association of Universities for Research in Astronomy, Inc., under NASA contract NAS 5-26555. These observations are associated with programs 7817, 9270, 9301, 9583, and 9803.
[3] Based on observations collected at the European Southern Observatory, Paranal, Chile (LP166.A-0701 and 169.A-045).
[4] Department of Physics, University of California, Santa Cruz, CA 95064; cdow@scipp.ucsc.edu.
[5] Department of Astronomy and Astrophysics, University of California, Santa Cruz, CA 95064; holden@ucolick.org, bouwens@ucolick.org, gdi@ucolick.org, magee@ucolick.org.
[6] Department of Physics and Astronomy, Johns Hopkins University, Baltimore, MD 21218-2686; wel@pha.jhu.edu, ford@pha.jhu.edu, azirm@pha.jhu.edu.
[7] Leiden Observatory, NL-2300 RA, Leiden, Netherlands; franx@strw.leidenuniv.nl.
[8] Department of Astronomy, Yale University, New Haven, CT 06520-8101; dokkum@astro.yale.edu.
[9] European Southern Observatory, D-85748 Garching, Germany; prosati@eso.org.

TABLE 1
PROPERTIES OF OUR RDCS 1252−2927 SPECTROSCOPIC SAMPLE

Object ID	Previous ID[a]	R.A.	Decl.	z_{850}	J	K_s	$i_{775} - z_{850}$	r_{hl} (arcsec)	z
BD 38[b,c]	1252-5224-4599	12 52 56.888	−29 25 55.50	24.3 ± 0.1	24.1 ± 0.1	23.8 ± 0.1	1.5	0.29	5.515
BD 03[b,c]	1252-2134-1498	12 52 45.382	−29 28 27.11	25.6 ± 0.1	25.2 ± 0.4	>25.6	>2.1	0.18	5.980
BD 27	...	12 52 51.902	−29 26 28.60	25.6 ± 0.1	26.1 ± 0.4	25.8 ± 0.4	1.5	0.11	...
BD 58	1252-2585-3351	12 52 52.283	−29 28 04.74	25.7 ± 0.1	25.6 ± 0.3	25.4 ± 0.3	2.0	0.20	...
BD 44	1252-5058-5920	12 53 01.745	−29 26 03.87	25.9 ± 0.2	26.3 ± 0.4	25.5 ± 0.4	>1.8	0.19	...
BD 46[b,d]	...	12 53 05.424	−29 24 26.22	26.1 ± 0.1	NA	NA	1.6	0.14	5.914
BD 57	...	12 52 49.441	−29 27 53.24	26.1 ± 0.2	25.7 ± 0.3	24.9 ± 0.2	1.5	0.19	...
BD 00[d]	...	12 52 42.927	−29 29 20.05	26.1 ± 0.1	NA	NA	1.3	0.11	5.942
BD 66	...	12 52 54.624	−29 24 56.18	26.1 ± 0.1	NA	NA	1.4	0.13	...
BD 40	...	12 52 59.511	−29 26 58.43	26.3 ± 0.1	26.2 ± 0.3	25.9 ± 0.4	1.3	0.15	...
BD 22	...	12 52 53.346	−29 27 10.58	26.5 ± 0.2	NA	NA	1.4	0.13	...
BD 62	1252-3729-4565	12 52 56.746	−29 27 07.63	26.7 ± 0.2	26.3 ± 0.3	>26.2	>1.8	0.12	...
BD 48	1252-3497-809	12 52 42.754	−29 27 18.89	27.0 ± 0.2	NA	NA	>1.6	0.11	...
BD 36	...	12 52 54.944	−29 25 57.52	27.1 ± 0.1	26.3 ± 0.4	25.2 ± 0.4	1.5	0.11	...

NOTES.—Right ascension (units of hours, minutes, and seconds) and declination (units of degrees, arcminutes, and arcseconds) use the J2000.0 equinox. All magnitudes given are AB. An entry of NA indicates that the object was outside the ISAAC coverage we had on Cl 1252 (Lidman et al. 2004). Each of these objects were observed for 4 hr with LRIS.

[a] Bouwens et al. (2003).
[b] FORS2 22.3 hr integrated spectra also obtained.
[c] Lacking detectable Lyα emission; absorption-line redshift.
[d] Lyα emission detected; emission-line redshift.

selection techniques, noting their respective strengths and complementarity. A brief outline of this paper follows. A summary of the *i*-dropout sample and spectroscopic observations is presented in § 2. In § 3 we present the spectra and their interpretations. In § 4 we compare our results with those obtained with narrowband selections at $z \sim 6$. In § 5 we discuss the fraction of LAEs in the *i*-dropout sample, as compared with lower redshift samples. We also investigate a possible link between the morphologies of the *i*-dropouts and their Lyα emission. Finally, in § 6 we summarize our findings and discuss their implications for future high-redshift surveys.

In this paper we adopt the "concordance" cosmology: a Λ-dominated, flat universe with $\Omega_M = 0.3$, $\Omega_\Lambda = 0.7$, and $H_0 = 71$ km s^{-1} Mpc^{-1} (Bennett et al. 2003). All magnitudes are given in the AB system (Oke & Gunn 1983). We denote the *Hubble Space Telescope* (*HST*) ACS F435W, F606W, F775W, and F850LP passbands as B_{435}, V_{606}, i_{775}, and z_{850}, respectively.

2. SAMPLE AND OBSERVATIONS

2.1. *Optical Broadband Dropout-selected Survey*

Our spectroscopic sample was derived from *HST* ACS observations over two separate fields: RDCS 1252.9−2927 (Cl 1252), a cluster at $z = 1.237$ selected from the *ROSAT* Deep Cluster Survey (Rosati et al. 1998, 2004), and the Ultra Deep Field parallel fields (UDF PFs; Bouwens et al. 2004a). A $6' \times 6'$ mosaic of ACS Wide Field Camera i_{775}- and z_{850}-band images was acquired around Cl 1252, with $4' \times 4'$ VLT ISAAC infrared (IR) imaging of the mosaic center (Lidman et al. 2004). The UDF PFs were imaged with a $4.5' \times 4.5'$ ACS mosaic in the B_{435}-, V_{606}-, i_{775}-, and z_{850}-band filters. For further details concerning the imaging data and our photometry over these fields, we refer the reader to Bouwens et al. (2003, 2004a).

The i_{775}- and z_{850}-band imaging data over these fields allow us to readily select LBGs in the range $5.5 < z < 6.2$ (Bouwens et al. 2003) using a *i*-dropout criteria. In the case of Cl 1252, the selection was based on a $i_{775} - z_{850} > 1.3$ color cut, and, for the UDF PFs (Bouwens et al. 2004a), on a $i_{775} - z_{850} > 1.4$ cut plus a null detection in V_{606} ($2\,\sigma$). Note that the color selection we use for following up sources in the Cl 1252 field is more inclusive than the $i_{775} - z_{850} > 1.5$ criterion used in Bouwens et al. (2003). The $i_{775} - z_{850} > 1.3$ criterion used for selection in the Cl 1252 field resulted from a small systematic error that was present in the early z_{850} ACS zero point. The typical error for the $i_{775} - z_{850}$ colors is 0.4 mag. In the case of a nondetection, the i_{775} flux was set to the $2\,\sigma$ upper limit. The error and upper limits are incorporated into all simulations that determine selection volume for the different samples. A total of 25 *i*-dropouts were identified in the Cl 1252 field, and 40 over the UDF PFs, with $10\,\sigma$ limiting magnitudes of $z_{850} = 27.3$ and 27.8, respectively. This corresponds to surface densities of 0.5 ± 0.1 objects arcmin^{-2} for Cl 1252 and 1.4 ± 0.2 objects arcmin^{-2} for the UDF PFs.

In Tables 1 and 2, the objects satisfying the *i*-dropout criteria for spectroscopic follow-up are listed, along with their z_{850}-band, J-band, and K_s-band magnitudes and their $i_{775} - z_{850}$ colors. A total of 22 objects were observed spectroscopically (14 in Cl 1252 and 8 in the UDF PFs). These objects were randomly selected from the entire *i*-dropout sample for spectroscopic follow-up, except for the most luminous dropout in the Cl 1252 field (BD 38), which was explicitly targeted for follow-up. In addition, *i*-dropout galaxies were the primary targets for both the Cl 1252 and UDF PF spectroscopic observations. The faintest galaxy on our mask had a z_{850}-band magnitude of 27.5.

2.2. *Keck I LRIS*

We used the Low Resolution Imaging Spectrograph (LRIS; Oke et al. 1995) on the Keck I 10 m telescope for spectroscopic follow-up of all 22 objects in our spectroscopic sample. A total integration time of 16,200 s for Cl 1252 objects and 7200 s for UDF PF objects was obtained using the 600 line mm^{-1} grating blazed at 8500 Å, with a slitlet width of $1''$ and a minimum slitlet length of $10''$. The scale ($\Delta\lambda_{res}$) of this configuration is 1.28 Å pixel^{-1}. A series of eight dithered exposures was taken to aid in cosmic-ray removal and to enhance removal of the fringing in the near-IR region of the spectra. The telescope was offset by $1''$–$3''$ along the slits between exposures, which ranged from

TABLE 2
PROPERTIES OF OUR UDF PARALLEL SPECTROSCOPIC SAMPLE

Object ID	Previous ID[a]	R.A. (J2000.0)	Decl. (J2000.0)	z_{850}	$i_{775} - z_{850}$	r_{hl} (arcsec)	z
UDF PFs1 i0	...	03 32 35.604	−27 57 37.51	25.5 ± 0.1	1.9	0.25	...
UDF PFs1 i1	...	03 32 34.892	−27 57 10.74	25.7 ± 0.1	1.5	0.11	...
GOODS i6 0[b]	...	03 32 39.803	−27 52 57.88	26.1 ± 0.1	1.4	0.10	5.540
UDF PFs i4[b]	UDFP1-3851-2438	03 32 43.959	−27 56 43.87	26.3 ± 0.1	1.6	0.11	5.857
UDF PFs i9	UDFP1-4650-3354	03 32 40.707	−27 57 24.28	26.4 ± 0.1	1.7	0.16	...
UDF PFs i1[b]	UDFP1-2954-1152	03 32 48.368	−27 55 54.82	26.9 ± 0.2	1.5	0.09	6.005
UDF PFs i2[b]	UDFP1-2309-1628	03 32 46.410	−27 55 24.32	27.1 ± 0.1	>2.5	0.10	6.083
UDF PFs i0[c]	UDFP1-3407-1028	03 32 48.952	−27 56 16.97	27.5 ± 0.2	1.7	0.10	...

NOTE.—Units of right ascension are hours, minutes, and seconds, and units of declination are degrees, arcminutes, and arcseconds.
[a] Bouwens et al. (2004a).
[b] Lyα emission detected.
[c] This object's LRIS spectrum was contaminated by bleeding from an alignment star spectrum. Therefore, it is excluded from the sample.

1200 to 2250 s in duration. The observations were taken under photometric conditions on the nights of UT 2004 February 13–14.

All data reductions were conducted using a slit mask reduction task developed by D. Kelson. This task yields cleaner background subtraction and cosmic-ray removal than standard slit spectroscopy procedures (Kelson 2003). By performing the sky subtraction before the data have been rectified, this methodology minimizes reduction errors. One example of this reduction procedure is presented in Figure 1. Wavelength calibration was performed using the night sky lines. The spectra were flux-calibrated using a sensitivity function derived from observations taken the same night of the spectrophotometric standard Hz 44 (Massey et al. 1988; Massey & Gronwall 1990).

2.3. *VLT FORS2*

Three Cl 1252 *i*-dropout objects (BD 38, BD 03, and BD 46) were also observed with the Focal Reducer and low dispersion Spectrograph 2 (FORS2) on the 8.2 m VLT Yepun Unit Telescope in mask exchange unit mode. These objects were observed as part of a large observing program aimed at acquiring very deep spectra of both field and cluster elliptical galaxies in the redshift range 0.6–1.3. We used the 600z grism with the OG590 order separation filter, which yielded a scale element of 1.64 Å pixel^{-1}. The data presented here were taken from UT 2003 February 28 through March 2 and from April 27 through May 24, with a median seeing of 0.65″ and clear conditions. The observations were carried out in a series of four dithered exposures with equal exposure times ranging from 14 to 30 minutes each, yielding a total integration time of 22.3 hr for the sources. All exposures are added and weighted such that optimal signal-to-noise ratios were obtained. Details concerning the data reduction are provided in van der Wel et al. (2005).

3. RESULTS

3.1. *Keck Data*

Six emission-line objects were detected out of the observed 22 object sample. No other spectral features were found (including continuum) in the remaining spectra. Figures 2*a*–2*f* show our spectra of these objects, with lines evident at 8440, 8404, 8514, 8609, 8335, and 7950 Å. Since O II λ3727 would be resolved into a doublet structure with our spectral resolution, this interpretation for these lines could clearly be rejected. Moreover, line interpretations as Hβ λ4861.3, Hα λ6562.8, and O III $\lambda\lambda$5006.8, 4958.9 could also be discarded due to the lack of nearby lines and the $i_{775} - z_{850} > 1.3$ colors (strong continuum breaks) of our objects. For objects BD 00, BD 46, UDF PFs i1, and UDF PFs i2,

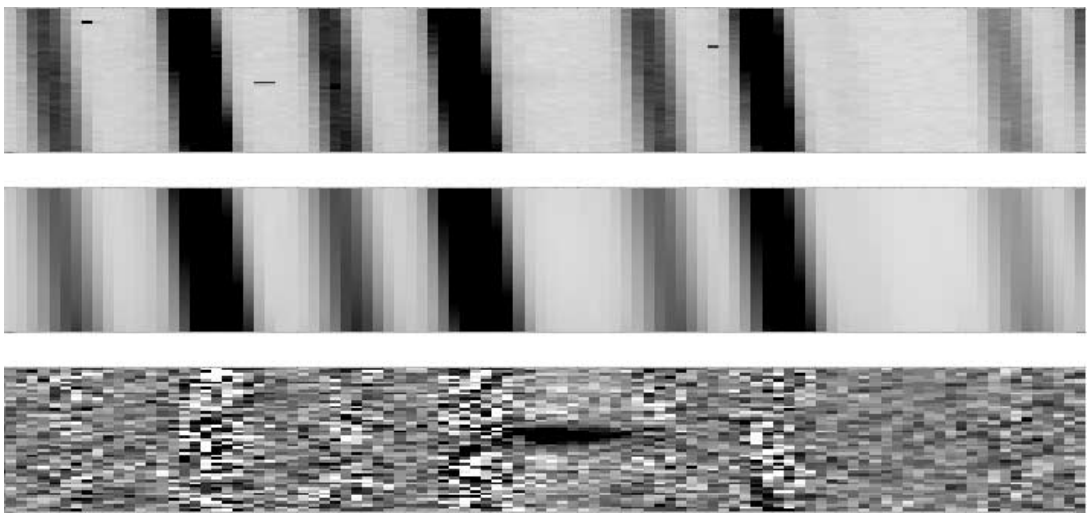

FIG. 1.—Illustration of the reduction process for our two-dimensional spectral data. The top panel shows the unreduced spectrum, the middle panel shows a two-dimensional fit to the background, and the bottom panel shows the reduced spectrum.

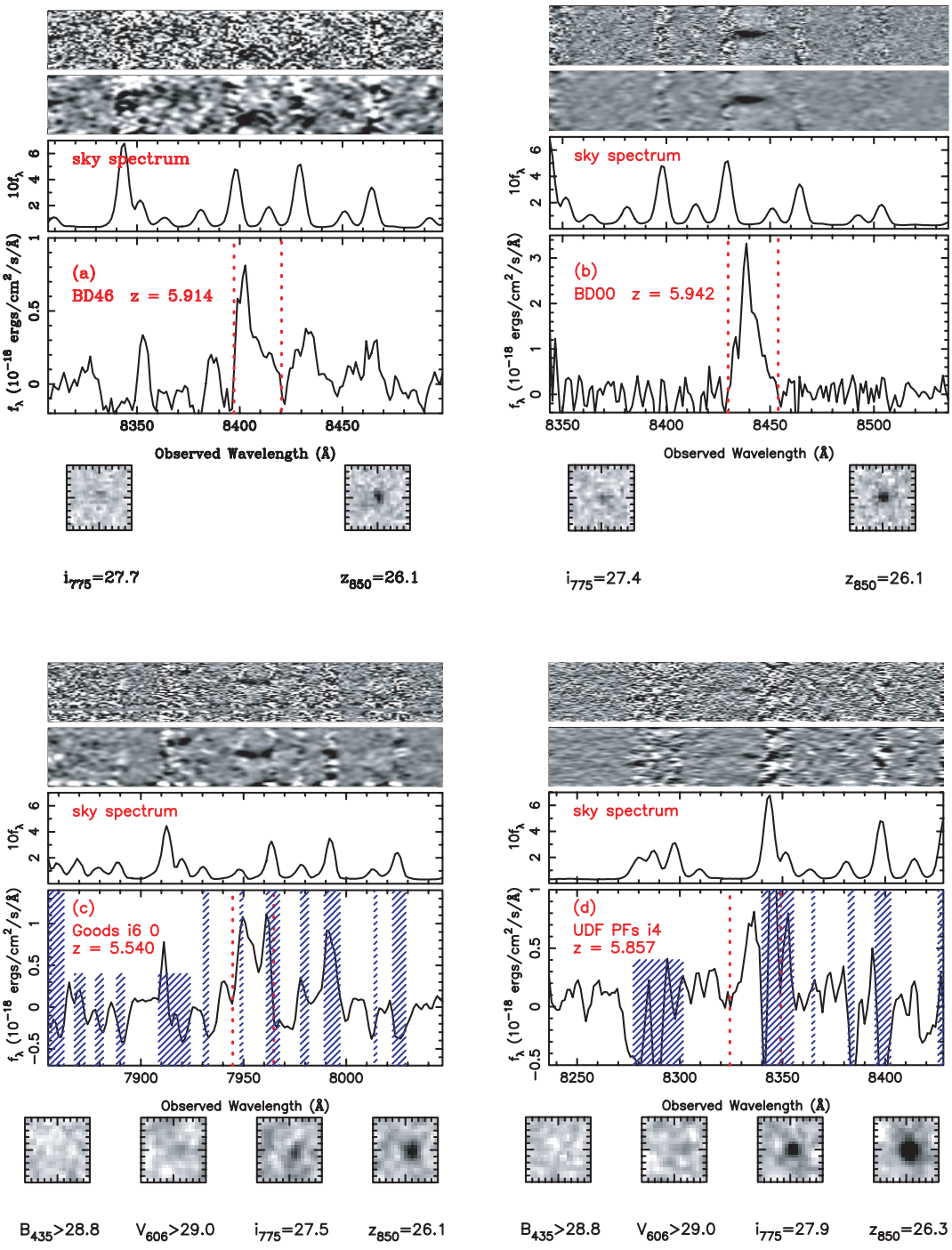

FIG. 2.—LRIS spectra and ACS imaging of emission-line objects: two-dimensional unsmoothed spectra (*top*), candidate Lyα emission (*bottom*), and ACS imaging (*postage stamps*). Also shown is the two-dimensional $\sigma = 1$ pixel Gaussian smoothed spectra of the sky (*middle*). Objects are (*a*) BD 46, (*b*) BD 00, (*c*) GOODS i6 0, (*d*) UDF PFs i4, (*e*) UDF PFs i1, and (*f*) UDF PFs i2. The postage stamps are $1.0'' \times 1.0''$. All upper limits given for the B_{453}-, V_{606}-, and i_{775}-band fluxes are 2 σ. The exposure times for the objects were 7200 s, except for the two Cl 1252 objects (BD 46 and BD 00), where the exposure times were 16,200 s. Each one-dimensional spectrum has been smoothed with a 3 pixel boxcar filter, except for BD 00 and BD 46. Vertical dotted lines delineate the region used for measuring line fluxes, equivalent widths, and FWHMs. For the UDF PFs objects, the blue hatched rectangles represent regions where strong sky lines are present. The $i_{775} - z_{850}$ colors and the asymmetry of these line profiles are consistent with the emission lines from BD 46, BD 00, UDF PFs i1, and UDF PFs i2 being Lyα λ1215.67. The other two emission-line objects (GOODS i6 0 and UDF PFs i4) are difficult to identify, due to sky line interference. We consider the implication that the features in these latter two sources are spurious and that Lyα is undetected.

the asymmetry of the line profiles, with absorption on the blue side, is consistent with absorption by a thick Lyα forest. Therefore, it seems quite clear that these emission lines are Lyα λ1215.67, placing these objects at $z = 5.942$, 5.9214, 6.005, and 6.083, respectively. For UDF PFs i4 and GOODS i6 0, the emission features are heavily contaminated by sky lines, making it difficult to ascertain their level of asymmetry and thus whether they are likely Lyα. We tentatively identify these emission features as Lyα, placing these objects at $z = 5.857$ and 5.540, respectively. However, in the discussion that follows, we also consider the implications that these objects are null detections or low-redshift contaminants.

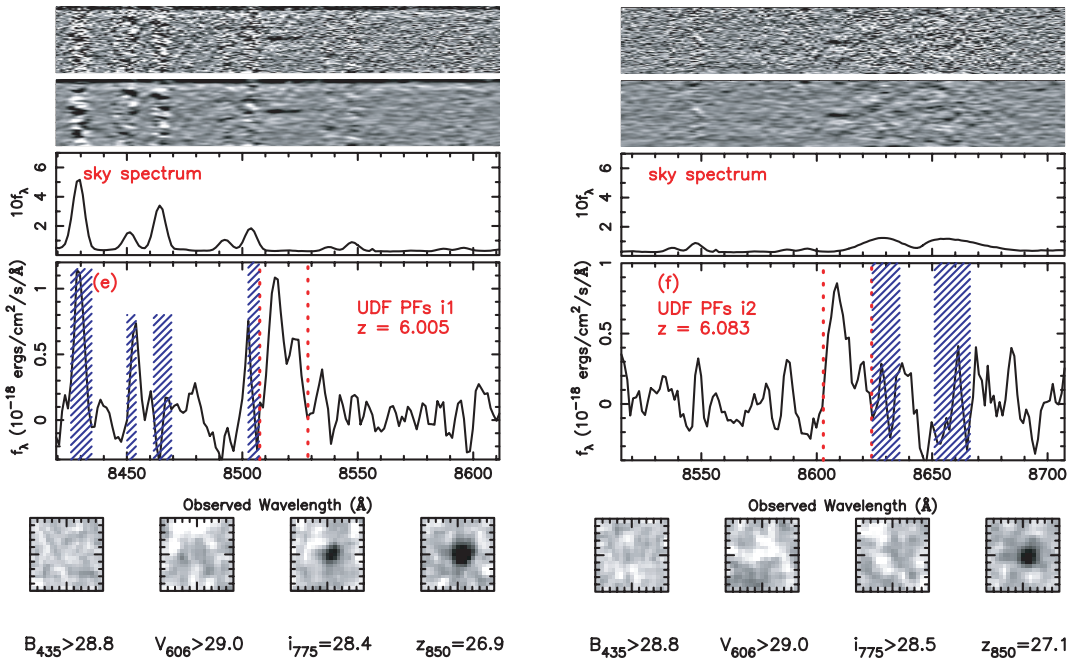

FIG. 2—*Continued*

To quantify the asymmetry of the four uncontaminated emission lines, we adopted the two asymmetry parameters developed by Rhoads et al. (2003). The "wavelength ratio," a_w, and the "flux ratio," a_f, are defined as

$$a_w = \frac{\lambda_{10,r} - \lambda_p}{\lambda_p - \lambda_{10,b}}, \quad (1)$$

$$a_f = \frac{\int_{\lambda_p}^{\lambda_{10,r}} f_\lambda \, d\lambda}{\int_{\lambda_{10,b}}^{p} f_\lambda \, d\lambda}, \quad (2)$$

respectively. Here λ_p is the wavelength of the peak of the emission, and $\lambda_{10,b}$ and $\lambda_{10,r}$ are the wavelengths where the flux exceeds 10% of its peak value on the blue and red sides of the emission, respectively. The resulting values, shown in Table 3, range from $a_w = 1.8$ to 2.6 and from $a_f = 1.4$ to 2.4. This is in agreement with values determined from Lyα-emitting objects at $z \approx 4.5$ (Dawson et al. 2004) and at $z \sim 5.7$ (Rhoads et al. 2003). These asymmetry parameters are inconsistent with those of the $z \approx 1$ O II λ3727 doublet ($a_w \leq 1$ and $a_f \leq 1$; Dawson et al. 2004). Note that for object BD 46, the FORS2 spectrum (see § 3.2.1) was used to calculate asymmetry parameters.

The spectrum of UDF PFs i0 was contaminated by bleeding from an alignment star, impeding detection of Lyα emission or a continuum. Thus, this object is excluded from our sample in the analysis below.

The two objects UDF PFs i1 ($z_{850} = 26.9$) and UDF PFs i2 ($z_{850} = 27.1$) are among the faintest $z > 5$ objects in the z_{850} band to be selected by the Lyman break technique with confirmed redshifts, very similar to the objects GLARE 3001 and 3011, with $z_{850} = 26.37 \pm 0.06$ and 27.15 ± 0.12, respectively (Stanway et al. 2004b). Furthermore, UDF PFs i2 is the faintest object in our sample (excluding UDF PFs i0) and is the object with the highest confirmed redshift.

Table 3 gives the measured redshifts, Lyα fluxes ($f_{\mathrm{Ly}\alpha}$), rest-frame equivalent widths ($W_{\mathrm{Ly}\alpha}$), and FWHMs of the six Lyα-emitting LBGs. We measured the flux in the emission lines between the red dotted lines illustrated in Figures 2 and 3. In some cases, there were residuals from the sky subtraction that could contaminate the line flux. We estimated this additional contribution from the sky lines by measuring the residual flux

TABLE 3
OBJECTS WITH DETECTABLE Lyα EMISSION

Object ID	z	$f_{\mathrm{Ly}\alpha}$[a,b] (10^{-17} ergs cm^{-2} s^{-1})	$W_{\mathrm{Ly}\alpha}$[b,c] (Å)	FWHM[b] (Å)	a_w[d]	a_f[d]
BD 46	5.914	0.90	24	6	1.9	1.8
BD 00	5.942	3.50	150	10	1.8	1.4
GOODS i6 0	5.540	1.34	31	19	...	...
UDF PFs i4	5.857	0.70	34	10	...	...
UDF PFs i1	6.005	1.10	65	13	2.6	2.4
UDF PFs i2	6.083	0.96	64	10	2.3	1.5

[a] Flux from Lyα emission.
[b] Not corrected for IGM absorption.
[c] Measured rest-frame equivalent width.
[d] Emission-line asymmetry parameters (Rhoads et al. 2003).

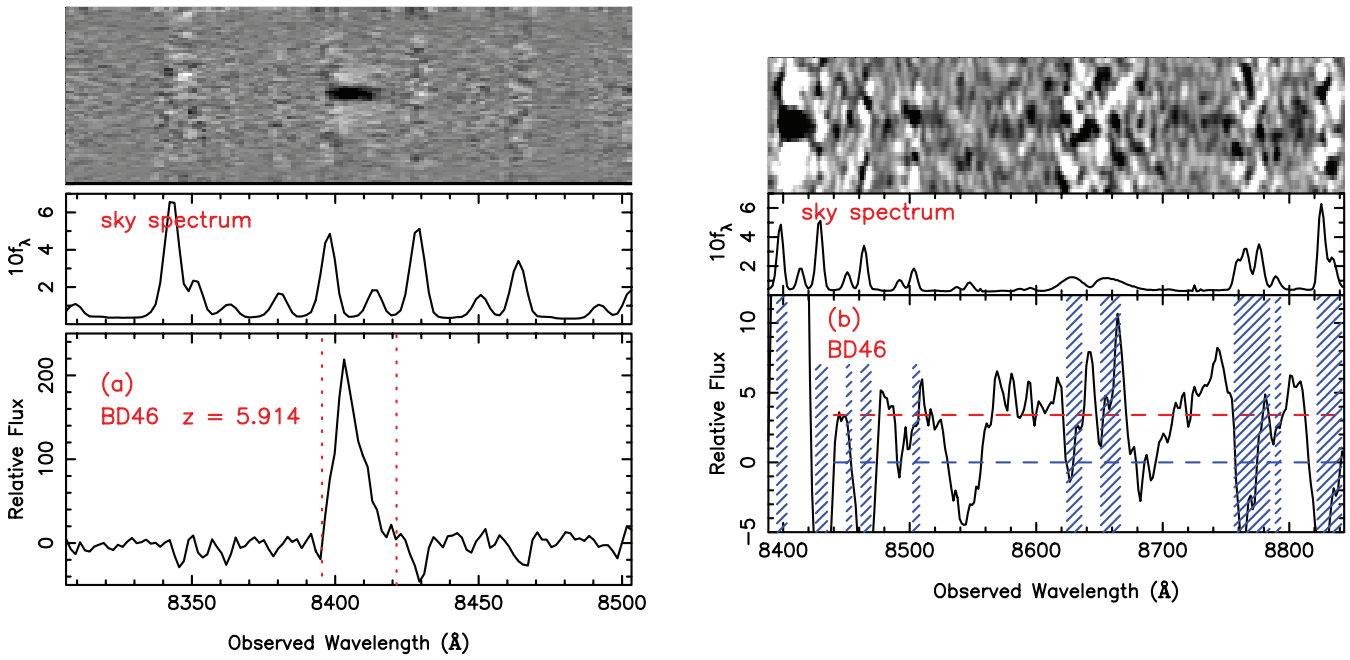

FIG. 3.—(*a*) FORS2 two- and one-dimensional spectra of BD 46 (LRIS spectrum shown in Fig. 2). The total exposure time is 22.3 hr. The Lyα emission occurs at 8406 Å, consistent with the LRIS spectrum. (*b*) Faint continuum of BD 46 redward of the emission. The two-dimensional spectrum has been smoothed with a $\sigma = 1$ Gaussian. The one-dimensional spectrum has been smoothed with a 10 pixel boxcar filter. The red dashed line delineates the continuum of $f = 3.4 \pm 1.0$ counts Å^{-1}.

in the two-dimensional sky-subtracted spectrum outside of the extraction region used for the one-dimensional spectrum. All values quoted were measured directly from the spectra, and they do not account for flux lost due to internal absorption in the objects. Therefore, the quoted fluxes are lower limits. The observed emission fluxes from our Lyα-emitting sample are very similar to those found for other $z \sim 6$ objects selected by the *i*-dropout method (Bunker et al. 2003; Stanway et al. 2004a, 2004b) and for $z \approx 5.7$ and $z \approx 6.6$ Lyα emitters selected using narrowband filters (Hu et al. 2004; Rhoads et al. 2003; Lehnert & Bremer 2003; Ajiki et al. 2003; Kurk et al. 2004; Taniguchi et al. 2005; Stern et al. 2005; Nagao et al. 2004; Rhoads et al. 2004). To determine the continuum for each spectrum, we assumed that it satisfied a power law of the form

$$f(\lambda) = f_0(\lambda/0.9\ \mu\mathrm{m})^{\beta}, \tag{3}$$

with $\beta = -1.1$, which is the average of 198 Lyα-emitting LBGs at $z \sim 3$ (Shapley et al. 2003). The quantity f_0 was determined by fitting the z_{850} magnitude. The equivalent widths of the Lyα emissions were calculated directly from these estimated continua. These widths were not very sensitive to the assumed value of β.

3.2. *VLT Data*

3.2.1. *BD 46*

The two-dimensional FORS2 spectrum of BD 46 showed a robust emission line at the central wavelength of 8406 Å. Two- and one-dimensional extracted spectra for this emission are shown in Figure 3*a*. A clear asymmetric profile for the line is seen, which we identify as Lyα, yielding a redshift of $z = 5.914$ for this source. Furthermore, a weak continuum was detected redward of the emission, with $f = 3.4 \pm 1.0$ counts Å^{-1}, as shown in Figure 3*b*. One item to note is that BD 46's Lyα emission was detected with LRIS before the VLT data were available. Our methodology accurately measured this redshift (it was within $\Delta z = 0.0005$ of the FORS2 value), despite a much weaker signal due to the smaller integration time in our Keck LRIS data.

3.2.2. *BD 03*

While this object was undetected in the LRIS (4 hr integration) spectrum, the FORS2 spectrum shown in Figure 4 contains a noisy but clearly flat continuum redward of 8500 Å, with a sharp discontinuity at 8485 ± 3 Å, where the flux drops to approximately zero blueward of 8400 Å. Using a constant step function to fit the continuum, we find that the average flux density above the discontinuity is $f^{\mathrm{red}}(8500\text{–}9100\ \text{Å}) = 5 \pm 1$ counts Å^{-1}. Below the break, this reduces to $f^{\mathrm{blue}}(7700\text{–}8300\ \text{Å}) = 1 \pm 1$ counts Å^{-1}, consistent with no detected flux.

This discontinuity is much larger than would be expected from UV/optical spectral breaks of galaxies at rest wavelengths 4000 Å [*D*(4000)], 2900 Å [*B*(2900)], and 2640 Å [*B*(2640)] (Stern et al. 2000; Spinrad et al. 1997, 1998). Another option is that this object could be a radio-loud broad absorption line quasar. Such objects can have large continuum breaks of this amplitude. However, such objects also possess very red near-IR colors (Hall et al. 1997), unlike BD 03 ($J - K_s < -0.03$). Furthermore, the resolved morphology of BD 03 is atypical for luminous active galactic nuclei (AGNs) at high redshift, which are generally unresolved.

The abruptness of the break and the lack of slope in the continuum at larger wavelengths are strong signs that the discontinuity is due to absorption by the intergalactic medium (IGM). Coupling this with the $i_{775} - z_{850} > 2.1$ colors (the second reddest in our spectroscopic sample), we interpret this object as being a starburst galaxy at $z = 5.98 \pm 0.1$. Using the LRIS spectrum, we place an upper flux limit of 8.0×10^{-19} ergs cm^{-2} s^{-1} on the Lyα emission.[10]

[10] All flux limits are for a 3 σ detection extracted over 4 Å ($\approx 3\Delta\lambda_{\mathrm{res}}$). Note that Stanway et al. (2004a) quoted a 10.5 hr DEIMOS spectra flux limit of 2.0×10^{-18} ergs cm^{-2} s^{-1}, which is for a 5 σ detection extracted over 8 Å.

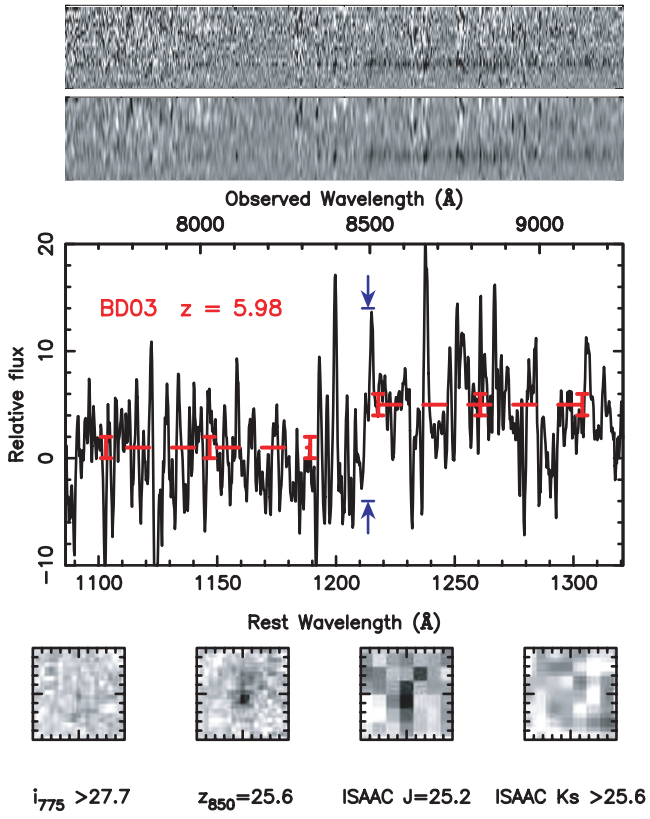

FIG. 4.—FORS2 spectra and ACS ISAAC imaging of BD 03 ($z = 5.98 \pm 0.1$). The upper two-dimensional spectrum is unsmoothed, while the lower one is smoothed with a $\sigma = 1$ pixel Gaussian. The extracted one-dimensional spectrum is smoothed with a 5 pixel boxcar filter. From left to right, the four postage stamp images are in the i_{775}, z_{850}, J, and K_s bands. The total exposure time is 22.3 hr. The lower axis of the bottom panel is the observed wavelength shifted to the systematic redshift $z = 5.98$. Blue arrows indicate the position of the continuum break. The dashed lines represent the wavelength region used to fit the continuum near the break, where error bars represent the 1 σ error.

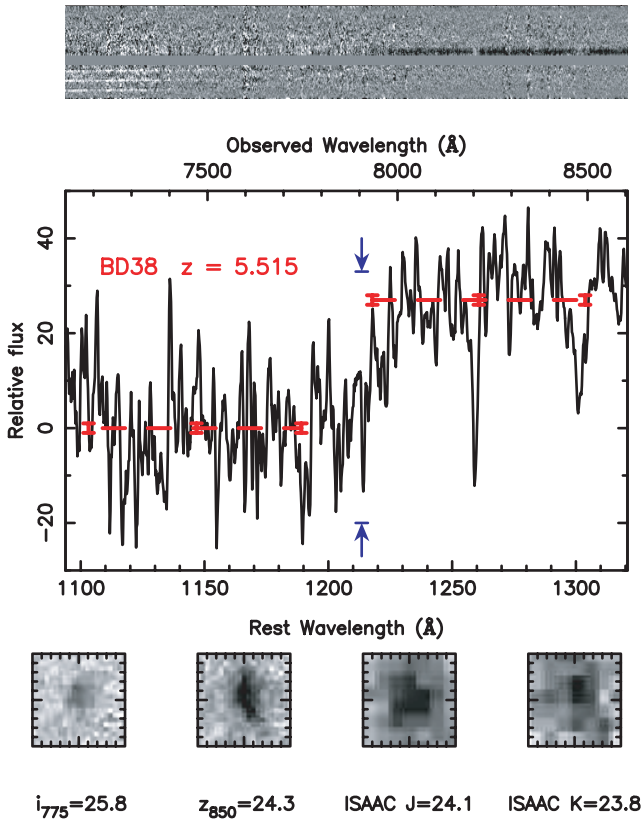

FIG. 5.—FORS2 spectra and ACS and ISAAC imaging of BD 38: two-dimensional spectrum and extracted one-dimensional spectrum smoothed with a 5 pixel boxcar filter. From left to right, the four postage stamp images are in the i_{775}, z_{850}, J, and K bands. The total exposure time is 22.3 hr. The lower axis of the bottom panel is the observed wavelength shifted to the systematic redshift $z = 5.515$. Blue arrows indicate the position of the continuum break. The dashed lines represent the wavelength region used to fit the continuum near the break, where error bars represent the 1 σ error. A more complete spectrum is shown in Dow-Hygelund et al. (2005).

3.2.3. *BD 38*

This object was also undetected in the LRIS observations, but it yields a strong continuum in the FORS2 spectrum. Figure 5 shows the two- and one-dimensional spectra of the object, along with the ACS and ISAAC imaging. A precipitous continuum break is clearly seen at ≈7900 Å, reducing the continuum from 27 ± 1 to 0 ± 1 counts Å^{-1}. Also, several strong absorption features are found at 8205.77, 8485.38, 8498.43, 8699.72, 9079.21, and 9140.84 Å in the spectrum. Associating the break with the UV optically thick Lyα forest and the absorption lines with the strong interstellar absorption features typical of LBGs at lower redshifts (see Shapley et al. 2003; Ando et al. 2004) yields a redshift determination of 5.515 ± 0.003.

BD 38 is an unusually bright i-dropout. Its z_{850}-band magnitude is 24.3, making this object more than 1.3 mag brighter than any other i-dropout in our spectroscopic or photometric sample. In fact, to our knowledge, this object is still the brightest $z \sim 6$ LBG discovered to date with a confirmed redshift. The complete spectrum, along with a more thorough analysis of this object, is presented in Dow-Hygelund et al. (2005).

4. DISCUSSION

4.1. *Confirmation and Contamination*

Of the total of 21 galaxies in our spectroscopic sample (excluding UDF PFs i0), we identified spectral features for eight objects. Of these eight, we confirmed that six i-dropouts from our sample are $z \sim 6$ galaxies, with the strong possibility that two more are. Therefore, the success rate of our survey is assuredly 29% and is most likely 38%. For the smaller integration times obtained with LRIS (4 hr), the completeness drops to 25% (19%, if we disregard GOODS i6 0 and UDF PFs i4). The confirmation rate in our longer 22.3 hr FORS2 integrations is 100% (3 out of 3). Interestingly, the two reddest $i_{775} - z_{850}$ color objects, the two brightest z_{850} objects, and the faintest z_{850} object in our sample are confirmed $z \sim 6$ galaxies.

There was no evidence from the spectra that any of the objects in our sample are low-redshift contaminants despite the long integration times. This is consistent with these objects being $z \sim 6$ continuum objects without strong Lyα emission. However, if we associate the emission lines of GOODS i6 0 and UDF PFs i4 with those of low-redshift interlopers (for which we have no evidence), the contamination of the sample could be as high as 14%, although this is unlikely. Support for this point is provided by the low-resolution spectroscopy conducted by Malhotra et al. (2005), using the ACS grism to test the i-dropout selection. Using a liberal color cut of $i_{775} - z_{850} > 0.9$ (versus our $i_{775} - z_{850} > 1.3$ criterion), they verified that 23 out of 29 candidate i-dropouts showed a strong continuum break indicative of galaxies at $z \sim 6$. In addition, they found that a color cut of $i_{775} - z_{850} > 1.3$, while suffering from modest (20%–30%) incompleteness, is subject to

a contamination rate of only 7% (1 out of 14).[11] Since the estimated contamination in the large (506 object) *i*-dropout selection of Bouwens et al. (2006) is similarly small ($\leq$8%), the present findings are perhaps not too surprising. This lends strong support to the notion that the objects in our sample without detectable features are primarily unconfirmed $z \sim 6$ galaxies and are not low-redshift interlopers.

To see if any of the unconfirmed galaxies in our Cl 1252 spectroscopic sample are low-z cluster members, we co-added the LRIS spectra associated with these sources in an effort to increase the signal-to-noise ratio (S/N) of the observations. If these objects were predominately $z = 1.23$ early-type contaminants, a break at $\approx$8800 Å would appear. No continuum break was detected in the co-added spectra, nor was any excess continuum found. Therefore, we concluded that the majority of the objects in our sample are not cluster members. We should note, however, that this null detection is not very surprising, considering that BD 38 and BD 03, which are the brightest objects in our sample and are confirmed $z \sim 6$ objects via the FORS2 observations, were undetected in the LRIS observations. The main conclusion of this analysis is that deeper spectroscopy is necessary to ascertain the nature of these galaxies.

4.2. *Star Formation Rate*

Aside from Lyα λ1215.67, no other emission lines were found in our sample of galaxies with Lyα emission. Another sometimes strong line in our wavelength range is the rest-frame UV line N v λ1240. This emission feature is strong in AGNs, with line ratios from a composite quasar spectra of $\langle f_{\mathrm{Ly}\alpha}/f_{\mathrm{N\,v}} = 4.0\rangle$ (Osterbrock 1989). The flux limits at rest-frame 1240 Å are $f_{\mathrm{N\,v}} < (0.8, 0.8, 1.0, 2.4, 2.2, 1.0) \times 10^{-18}$ ergs cm^{-2} s^{-1}, implying lower limits of the $f_{\mathrm{Ly}\alpha}/f_{\mathrm{N\,v}} > (11.3, 44.8, 13.4, 2.9, 5.0, 9.6)$ line ratios. Furthermore, no object in our sample was detected in *Chandra* or *XMM-Newton* X-ray imaging data (Rosati et al. 2004; Giacconi et al. 2002). The lack of any N v λ1240 emission or X-ray detection suggests that the Lyα emission is not produced by an AGN. Thus, we believe that the Lyα photons are primarily from hot young stellar populations, consistent with the Lyα-emitting objects being starbursting galaxies.

Now we estimate the star formation rates of the 8 confirmed and 13 unconfirmed objects in our $z \sim 6$ sample. Two different methods are used, the first relying on the Lyα emission flux ($\mathrm{SFR}_{\mathrm{Ly}\alpha}$) to make this estimate, and the second relying on the UV continuum flux ($\mathrm{SFR}_{\mathrm{UV}}$). The relationship between the Lyα flux and the SFR of a galaxy is given by

$$\mathrm{SFR}_{\mathrm{Ly}\alpha} = 9.1 \times 10^{-43} L_{\mathrm{Ly}\alpha}\ M_{\odot}\ \mathrm{yr}^{-1}, \quad (4)$$

where $L_{\mathrm{Ly}\alpha}$ is the Lyα luminosity in units of ergs s^{-1}, assuming a Salpeter initial mass function with $(m_{\mathrm{lower}},\ m_{\mathrm{higher}}) = (0.1\ M_{\odot},\ 100\ M_{\odot})$ (Salpeter 1955; Brocklehurst 1971; Kennicutt 1998). The SFRs determined by this method yield lower limits, due to absorption of Lyα photons by dust grains within the galaxy and by the Lyα forest (Hu et al. 2002). The SFRs can also be derived from the UV continuum luminosities (L_{UV}) at $\lambda = 1500$ Å, using the following relation:

$$\mathrm{SFR}_{\mathrm{UV}} = 1.4 \times 10^{-28} L_{\mathrm{UV}}\ M_{\odot}\ \mathrm{yr}^{-1}, \quad (5)$$

where L_{UV} is in units of ergs s^{-1} Hz^{-1} (Madau et al. 1998). For the nine objects with ISAAC imaging, the slope of the continuum was derived from the z_{850}, J, and K_s magnitudes, assuming that the UV spectrum can be described by $f_{\lambda} \propto \lambda^{\beta}$. The continuum slope used for the remaining objects was the consistent value of $\beta = -2.0$ found from *HST* NICMOS imaging of 26 *i*-dropout objects in the UDF (Stanway et al. 2005; Bouwens et al. 2006). We adopted a different value of β than that used in § 3.1 because of the observed β dependence on Lyα emission strength at $z \sim 3$ (Shapley et al. 2003). For the objects in our sample for which we cannot measure redshifts, the mean redshift for *i*-dropouts in our selection, $z = 5.9$ (Bouwens et al. 2003), is assumed.

For objects in the Cl 1252 field, we used the results of Lombardi et al. (2005) to correct for gravitational amplification by the cluster potential. For each object, we assumed a non–singular isothermal sphere lensing model with a free central position. This yields a best-fit velocity dispersion of 1185 km s^{-1}. Again, for the nondetected objects, the mean redshift $z = 5.9$ was used. The resulting gravitational magnifications are presented in the second column of Table 4. Most objects are two or more Einstein radii away, being only weakly lensed. However, BD 22 and BD 62 are close to the Einstein radius, and therefore the magnifications quoted for these sources are highly uncertain. Hereafter only delensed values for objects in the Cl 1252 field are quoted, except for BD 22 and BD 62, for which observed values are retained.

In Table 4 we present $L_{\mathrm{Ly}\alpha}$, L_{UV}, $\mathrm{SFR}_{\mathrm{Ly}\alpha}$, and $\mathrm{SFR}_{\mathrm{UV}}$ for the Lyα-emitting objects in our sample. Errors in L_{UV} and $\mathrm{SFR}_{\mathrm{UV}}$ are derived from the z_{850}-band flux errors. As is seen elsewhere (Hu et al. 2002; Kodaira et al. 2003; Ajiki et al. 2003), for the five Lyα-emitting objects, the ratio of $\mathrm{SFR}_{\mathrm{Ly}\alpha}$ to $\mathrm{SFR}_{\mathrm{UV}}$ ranges widely, from 27% to 127%. This is most likely due to absorption of Lyα photons by the IGM (Hu et al. 2002).

4.3. *Selection Completeness for* Lyα *Emitters*

Lyα λ1215.67 emission is by far the most prominent spectral feature we can use for redshift determination of $z > 5$ objects. When the Lyα emission is strong, it can have an effect on the observed broadband fluxes. At $z < 6$, Lyα flux falls in the *i* band, yielding $i - z$ colors that are smaller than those of objects without such emission. This effect is notable in Figure 6, where we show the $i_{775} - z_{850}$ colors versus the z_{850}-band magnitudes of our sample. Aside from UDF PFs i2, which is at $z = 6.083$, the Lyα-emitting objects inhabit the region $i_{775} - z_{850} \leq 1.6$. Moreover, from Vanzella et al. (2006, 2005), Dickinson et al. (2004), Nagao et al. (2004), Stanway et al. (2004a, 2004b), Bunker et al. (2003), and this work, only two confirmed Lyα-emitting objects have been detected by the *i*-dropout technique for $z < 5.78$. Once Lyα redshifts into the z_{850} band, the decrement can be larger than it would be without emission, such as for the $z = 6.33$ Lyα-emitting *i*-dropout object SDF J132440.6+273607 discovered by Nagao et al. (2004).

In Figure 7, we present the redshift distribution of spectroscopically confirmed $z \sim 6$ *i*-dropouts. The top histogram contains objects from this work and from Stanway et al. (2004a, 2004b), Malhotra et al. (2005), and Vanzella et al. (2006). The bottom histogram only contains those objects that have measurable Lyα emission. In addition, the expected distribution of *i*-dropouts from the simulations of Bouwens et al. (2003, 2006) are plotted. From these curves it is evident that as the strength of Lyα emission increases, the mean redshift of the *i*-dropout population increases quite noticeably, while the width of this

[11] This contaminant was a star. The methodology of Bouwens et al. (2003, 2004a, 2006) uses the SExtractor stellarity parameter (Bertin & Arnouts 1996) to exclude stars from our *i*-dropout selection. Hence, this contaminant would likely have been rejected from our spectroscopic sample. Thus, our null contamination results are consistent with the findings of Malhotra et al. (2005).

TABLE 4
STAR FORMATION RATES FOR OUR $z \sim 6$ SAMPLE

Object ID	μ[a]	$L_{Ly\alpha}$[b] ($10^{42}\ h_{0.7}^{-2}$ ergs s^{-1})	L_{UV}[c] ($10^{28}\ h_{0.7}^{-2}$ ergs s^{-1} Hz^{-1})	SFR$_{Ly\alpha}$[d] ($h_{0.7}^{-2}\ M_\odot$ yr^{-1})	SFR$_{UV}$[e] ($h_{0.7}^{-2}\ M_\odot$ yr^{-1})
BD 38	1.3	<0.5[f]	27.1 ± 2.7	<0.5	38.1 ± 3.8
BD 03	1.2	<0.3[f]	10.0 ± 1.0	<0.4	13.4 ± 1.3
BD 00	1.1	13.24	6.8 ± 0.7	12.1	9.5 ± 1.0
BD 46	1.1	3.37	6.7 ± 0.7	3.1	9.5 ± 1.0
GOODS i6 0	...	4.31	6.7 ± 0.7	3.9	9.4 ± 1.0
UDF PFs i4	...	2.56	6.1 ± 0.6	2.3	8.5 ± 1.0
UDF PFs i1	...	4.27	3.5 ± 0.7	3.9	5.1 ± 1.0
UDF PFs i2	...	3.84	3.1 ± 0.3	3.5	4.3 ± 0.4
UDF PFs i0	...	NS	12.9 ± 1.3	...	18.0 ± 1.8
UDF PFs-IDROP1	...	NS	12.9 ± 1.3	...	18.0 ± 1.8
BD 27	1.5	NS	7.6 ± 0.8	...	10.6 ± 1.1
BD 44	1.2	NS	7.3 ± 1.5	...	10.1 ± 2.0
BD 58	1.6	NS	6.6 ± 0.7	...	9.3 ± 1.0
BD 66	1.2	NS	6.2 ± 0.6	...	8.67 ± 0.9
UDF PFs1 i9	...	NS	5.6 ± 0.6	...	7.9 ± 0.8
BD 57	1.3	NS	5.3 ± 1.1	...	7.7 ± 1.5
BD 22	4.22	NS	5.1 ± 1.0[g]	...	7.2 ± 1.4[g]
BD 62	35.1	NS	4.1 ± 0.8[g]	...	6.2 ± 1.2[g]
BD 40	1.6	NS	3.9 ± 0.4	...	5.4 ± 0.5
BD 48	1.2	NS	2.7 ± 0.5	...	3.8 ± 0.8
BD 36	1.4	NS	2.4 ± 0.2	...	3.4 ± 0.3

NOTES.—Uncertainties in L_{UV} and SFR$_{UV}$ are derived from the z_{850}-band flux errors. All quoted luminosities and star formation rates for Cl 1252 cluster objects are corrected for possible lensing, except for BD 22 and BD 62, for which the observed values are used. An entry of "NS" indicates that no spectral features were detected for the object. Where no redshift could be determined, the quoted UV luminosities are for the object at the mean redshift of $z = 5.9$ estimated for the *i*-dropout selections (Bouwens et al. 2003).

[a] Gravitational magnification due to the Cl 1252 cluster potential.
[b] Lyα luminosity.
[c] UV continuum luminosity at $\lambda = 1500$ Å.
[d] SFR derived from $L_{Ly\alpha}$.
[e] SFR derived from L_{UV}.
[f] No detectable Lyα emission.
[g] Not corrected for gravitational lensing and thus highly uncertain.

distribution narrows somewhat. Hence, there is a substantial bias against lower redshift ($z \lesssim 5.7$), strong ($W_{Ly\alpha} \geq 50$ Å) Lyα-emitting *i*-dropouts being selected as *i*-dropouts. However, this effect is small for weaker ($W_{Ly\alpha} = 25$ Å) Lyα-emitting objects. Considering that over half of the Lyα-emitting objects in our sample have $W_{Ly\alpha} \leq 30$ Å, this should only result in a modest bias. In § 5.1 we discuss this issue further.

To understand how Lyα emission affects *i*-dropout selection and how this influence evolves with redshift, we modeled the spectra of the Hu et al. (2004, hereafter Hu04) sample of 19 confirmed $z \approx 5.7$ LAEs, all identified by a narrowband selection. We plot the colors for Hu04 in Figure 8. Spectra of these objects were assumed to satisfy the power law given in equation (3). The flux decrement due to the IGM was modeled as a simple transmission coefficient, where initial values for the fit were obtained from the tables of Songaila (2004). The continuum level was set to zero blueward of the Lyman limit at 912 Å. The IGM transmission, f_0, and total Lyα emission integrated flux were varied as three fit parameters until the quoted NB$_{8150}$, Cousins *Z*, and Cousins *I* magnitudes in Hu04 were reproduced using the IRAF software package Synphot. These fiducial spectra were then artificially redshifted or blueshifted across the space probed by the i_{775}-dropout technique in intervals of $\Delta z = 0.1$. At each interval, the i_{775} and z_{850} magnitudes were recomputed using the model for each galaxy.

By directly applying our search criterion on these calculated i_{775} and z_{850} magnitudes, we can determine the efficiency of the i_{775}-dropout method at selecting LAEs at various redshifts. We use the relation

$$n = \int_{z_1=5.5}^{z_2=6.2} \rho(z)\, dV(z) \approx \sum_{i=1}^{7} \rho(z_i)\Delta V(z_i) = \sum_{i=1}^{7} \bar{\rho}\epsilon(z_i)\Delta V(z_i), \quad (6)$$

where n is the expected value of the LAEs, $\rho(z)$ is the volume density of the Hu04 LAEs at redshift z, $\bar{\rho}$ is the true volume density of the Hu04 objects, $\epsilon(z_i)$ is the fraction of the Hu04 LAEs that we would select at redshift z_i (i.e., selection probability), $\Delta V(z_i)$ is the volume element for the redshift interval $\Delta z = 0.1$, and the sum ranges from $z_1 = 5.5$ to $z_7 = 6.1$, approximating the integral from $z = 5.5$ to $z = 6.2$. This relation yields an expectation value of 3.0 strong LAEs in the Cl 1252 field.

This expectation value is an upper limit because of two additional effects. First, the probability of a $z \sim 6$ object being selected by the $i_{775} - z_{850}$ dropout technique is a strong function of redshift, dropping off rapidly at the highest redshifts probed (Bouwens et al. 2003, 2006). This is due to surface brightness selection effects that are at work at the high-redshift end of our $z \sim 6$ *i*-dropout selection (see Bouwens et al. 2006). Second, Lyα emission redshifted into the OH bands will be

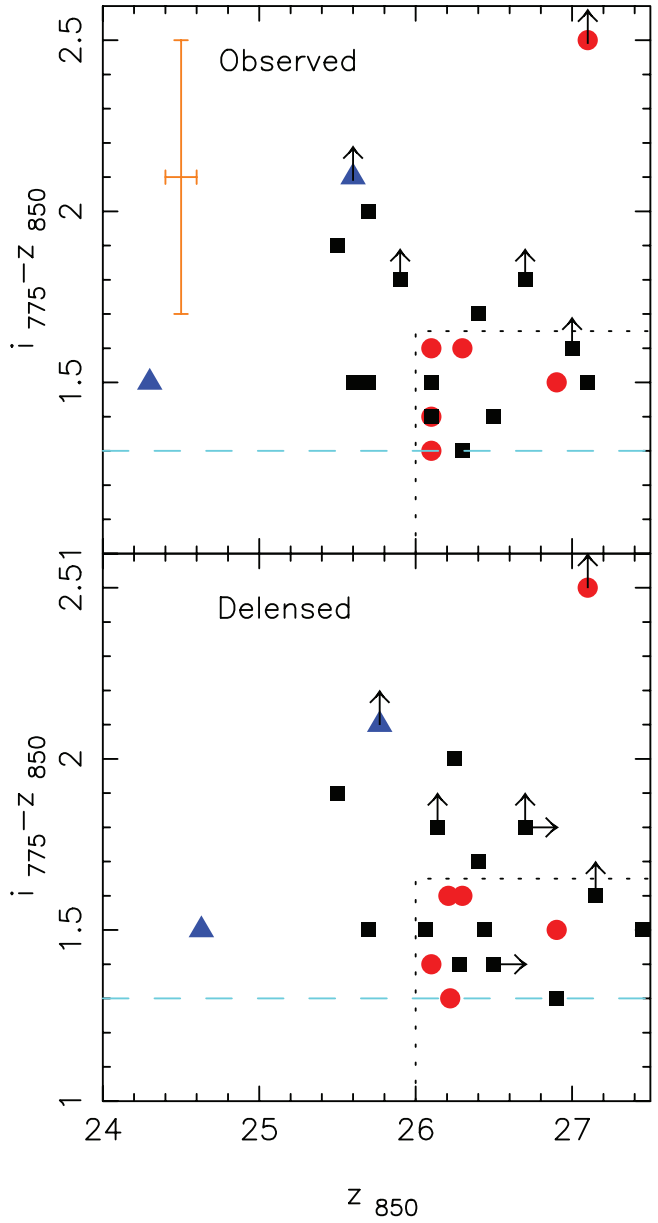

FIG. 6.—Observed (*top*) and delensed (*bottom*) $i_{775} - z_{850}$ colors vs. z_{850}-band magnitudes for our spectroscopic sample. The black squares represent sources where no spectral features were found, red circles indicate sources with Lyα emission, and blue triangles represent the sources with no detectable Lyα emission but for which we can derive a redshift (BD 03 and BD 38). Objects undetected in the i_{775} band are shown at their 2 σ lower limits and include upward-pointing arrows. The sources in Cl 1252 that are not delensed are shown with right-pointing arrows. The top left orange error bars are those typical for objects detected in the i_{775} filter. Our $i_{775} - z_{850} > 1.3$ selection criterion is denoted with the blue dashed line. Aside from UDF PFs i2, the distribution of Lyα emitters is constrained to $z_{850} \geq 26.1$ and $i_{775} - z_{850} \leq 1.6$ (demarcated by dotted lines). In the observed plot, almost half of the objects (9 out of 21) lie outside this region. However, this trend is absent after delensing the objects. Lyα-emitting objects likely have bluer $i_{775} - z_{850}$ colors than other *i*-dropouts as a result of the contribution of Lyα flux to the i_{775}-band magnitudes (see Fig. 7).

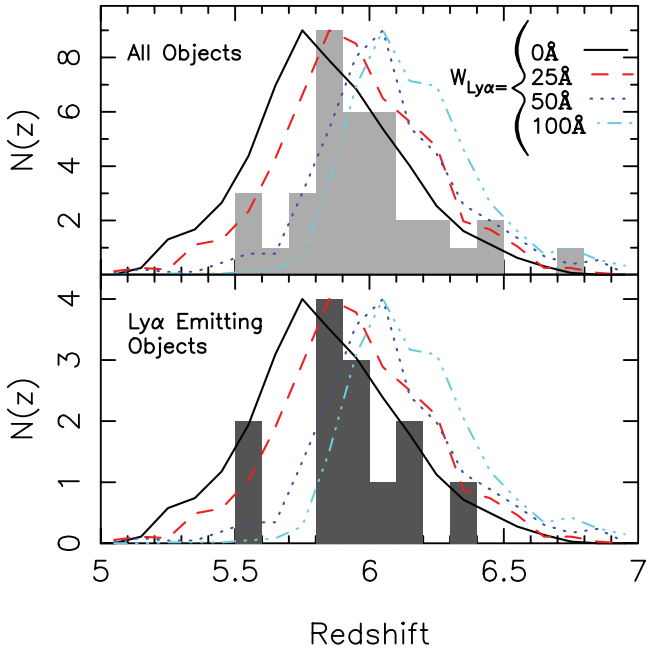

FIG. 7.—Observed distribution of spectroscopically confirmed $z \sim 6$ *i*-dropouts ($i_{775} - z_{850} > 1.3$). The top histogram contains confirmed sources from this work and from Stanway et al. (2004a), Stanway et al. (2004b), Malhotra et al. (2005), and Vanzella et al. (2006). The bottom histogram contains objects with detectable Lyα emission. Overplotted are simulated redshift distributions for four different Lyα equivalent widths $W_{\rm Ly\alpha}$, indicating the impact of these equivalent widths on the redshift distribution of the *i*-dropout selection. Overall, the simulations respectably encompass the observed distribution and suggest that most star-forming galaxies at $z \sim 6$ only have modest Lyα equivalent widths.

much more difficult to detect than emission in the region between the bands, and so the comoving volume probed will be smaller than we assumed. This is mitigated by the fact that the quoted flux limit of Hu04 is 2×10^{-17} ergs cm^{-2} s^{-1}. This is slightly greater than the average flux limit for our Cl 1252 spectra for Lyα emission in the redshift interval probed (1.9×10^{-17} ergs cm^{-2} s^{-1}).

Hence, we believe the expectation value of 3.0 LAEs to be consistent with our spectroscopic results of two Lyα-emitting LBGs (BD 00 and BD 46) in our Cl 1252 sample of 12 objects. Moreover, it appears that our survey is complete in selecting Lyα flux from objects that have measurable Lyα emission. Coupling this with our likely minimal low-redshift contamination rates (see § 4.1) suggests that Lyα-emitting LBGs only represent a fraction of the *i*-dropout–selected $z \sim 6$ LBGs.

We also estimated the total number of expected LAEs, assuming no evolution in the Hu04 sample. The Hu04 volume density translates into a surface density of 0.21 objects arcmin^{-2}. Making the somewhat crude assumption that an *i*-dropout selection of the Hu04 LAEs is similar to the Bouwens et al. (2003) *i*-dropout selection across the entire redshift interval probed implies that 40% of the latter sample are LAEs. This yields a strict upper limit of 5.6 expected LAEs in our Cl 1252 sample. From this, the *i*-dropout selection misses 46% of the total LAE population, although most of those missed are at the low-redshift end of the *i*-dropout range.

5. TRENDS IN $z \sim 6$ LYMAN BREAK GALAXIES

5.1. *Fraction of* Lyα*-emitting Galaxies*

In our sample, we find six objects (four if GOODS i6 0 and UDF PFs i4 are disregarded) with rest-frame equivalent widths strong enough to be detected as narrowband excess objects ($W_{\rm Ly\alpha} \geq 20$ Å). Thus, 29% (19%) of our sample (excluding UDF PFs i0) would be recovered by narrowband surveys. Similar results of 33%, 33%, and 31% are found by Stanway et al. (2004a), Stanway et al. (2004b), and Vanzella et al. (2006). These observations, and the results of the Lyα emission completeness test of § 4.3, suggest that Lyα-emitting objects represent ≈30% of *i*-dropout spectroscopic samples.

However, just because the fraction of *i*-dropouts with Lyα emission is 30% does not imply that the same thing is true for the

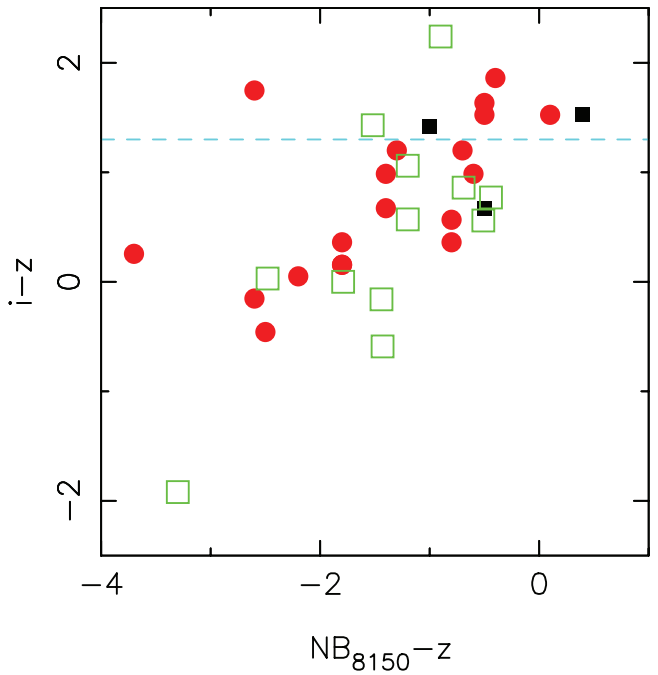

FIG. 8.—Color-color ($i - z$ vs. $NB_{8150} - z$) distribution of two narrowband-selected samples. The red circles show spectroscopically confirmed $z \approx 5.7$ Lyα emitters, and the black filled squares represent unconfirmed objects from Hu04. The green open squares represent narrowband-excess candidate Lyα emitters from Ajiki et al. (2006). No excess flux in the z_{850} band was measured for two objects in this sample; hence, they are excluded from the plot. A typical i-dropout color selection of $i_{775} - z_{850} > 1.3$ is shown by the blue dashed line. Nine out of 33 objects are within our selection limits. Hence, the i-band dropout technique seems to select ≈30% of the $z \approx 5.7$ Lyα emitters found by narrowband surveys. It is relevant to note that four of these are the weakest emitters of the confirmed sample of Hu04. The other objects do not meet our selection criterion because of the contribution of Lyα flux to the i-band magnitude (see Fig. 7). As noted in Fig. 7, this selection bias is not a problem for higher redshift ($z \geq 6$) LAEs.

$z \sim 6$ population as a whole. In § 4.3, and as can be easily seen in Figure 7, the $i_{775} - z_{850} > 1.3$ color cut biases our selection against the inclusion of lower redshift ($z < 5.8$) objects with strong Lyα emission (≥50 Å). This suggests that the effective selection volumes (and redshift distributions) of i-dropouts with significant Lyα emission may be quite different from the distribution without such emission.

This can be accounted for by using the simulations of Bouwens et al. (2006; see Fig. 7) to determine the effective search volumes, and the corresponding densities, for objects of different Lyα equivalent widths. For the distribution of $W_{Ly\alpha}$ in our sample (i.e., three objects with $W_{Ly\alpha} = 25$ Å, two with $W_{Ly\alpha} = 50$ Å, and one with $W_{Ly\alpha} = 100$ Å), these simulations imply that 32% ± 10% of star-forming galaxies at $z \sim 6$ have $W_{Ly\alpha} \geq 20$ Å, and 7% ± 6% have $W_{Ly\alpha} \geq 100$ Å.[12] In the situation in which every Lyα-emitting object in our sample has $W_{Ly\alpha} = 100$ Å and spectroscopy misses every object with $z \geq 6.15$, this fraction increases to 46% ± 11%. This case is an upper limit, given our assumptions. A lower limit of 25% ± 10% is determined if the emission-line objects GOODS i6 0 and UDF PFs i4 are lower redshift contaminants. A similar Lyα-emitting fraction of 32% ± 14% (upper limit of 47% ± 16%) is found using the results of Stanway et al. (2004a).

These results are similar to those obtained from Shapley et al. (2003), who analyzed spectra of over 1000 $z \sim 3$ LBGs. Although Shapley et al. (2003) selected their LBGs photometrically using a two-color cut, the extra color is used to remove potential low-redshift contaminants. As noted in § 4.1, the expected contamination of our survey is small; hence, we believe that our $z \sim 6$ LBG survey is similar enough to warrant comparison. Shapley et al. (2003) find that only 25% of their sample of $z \sim 3$ LBGs have $W_{Ly\alpha} \geq 20$ Å, and ∼2% have $W_{Ly\alpha} \geq 100$ Å. This is similar to the value we determine from our observed Lyα fraction (as well as that of Stanway et al. 2004a). Moreover, the fraction of $z \sim 3$ objects with $W_{Ly\alpha} \geq 20$ Å is within 2 σ of our $z \sim 6$ upper limit. Therefore, it appears that there is no strong evolution in the fraction of Lyα-emitting objects between $z \sim 3$ and $z \sim 6$.

Differing results are found by Shimasaku et al. (2006), who compare the $z \sim 6$ LBG luminosity function of Bouwens et al. (2006) with that derived from their $z \approx 5.7$ LAE sample. These authors determine that nearly every $z \sim 6$ LBG with $M_{UV} \lesssim -20$ ($z_{850} \lesssim 26.6$ mag) should have $W_{Ly\alpha} \geq 20$ Å. In fact, Shimasaku et al. (2006) argue that the fraction of $z \sim 6$ LBGs with $W_{Ly\alpha} \geq 100$ Å is ≈80%. Clearly, these results are inconsistent with our analysis above. At best, the Shimasaku et al. (2006) fraction is a factor of ≈2 too high. To be consistent with our survey, the spectroscopic efficiency we calculated in § 4.3 must be a factor of >10 too low, a situation we consider highly unlikely, given our agreement with the results of Hu04 and Stanway et al. (2004a). Hence, we believe that the Lyα-emitting fraction of nearly unity found by Shimasaku et al. (2006) must be wrong. This may be partially due to the mild evolution in the luminosity function that occurs between $z \approx 5.9$ (the mean redshift of the Bouwens et al. [2006] i-dropout selection) and $z \approx 5.7$, which is not accounted for by Shimasaku et al. (2006).

5.2. *Luminosities and Star Formation Rates*

Objects in our sample with measurable Lyα emission all have observed z_{850}-band magnitudes of 26.1 or fainter, populating the faintest 70% of the top panel of Figure 6. Furthermore, the brightest two objects in our Cl 1252 sample were confirmed $z \sim 6$ LBGs without any detectable Lyα emission. However, after delensing the sources in our Cl 1252 sample (Fig. 6, *bottom*), this luminosity segregation of Lyα-emitting objects is removed. The Lyα-emitting LBGs found by Stanway et al. (2004a) have z_{850}-band magnitudes of 25.48 ± 0.03, 26.37 ± 0.06, and 27.15 ± 0.12. Aside from the brightest object in the Stanway et al. (2004a) sample and the extremely bright ($z_{850} = 24.7$) object of Bunker et al. (2003), all confirmed $z \sim 6$ Lyα-emitting i-dropout objects have z_{850}-band magnitudes in excess of 26.

The average star formation rate derived from the UV continuum (SFR_{UV}) of our entire sample (excluding the $6L^*$ object BD 38) is $8.8 \pm 3.9\ h_{0.7}^{-2}\ M_\odot\ yr^{-1}$. This value increases slightly to $9.2 \pm 4.4\ h_{0.7}^{-2}\ M_\odot\ yr^{-1}$ if we exclude Lyα-emitting objects. The average SFR_{UV} of Lyα-emitting objects is $7.7 \pm 2.2\ h_{0.7}^{-2}\ M_\odot\ yr^{-1}$. Hence, the SFR_{UV} of Lyα-emitting objects appears to be similar to that of the i-dropout population in general; see Figure 9. Shapley et al. (2003) find at $z \sim 3$ that Lyα-emitting galaxies with stronger Lyα emission have lower star formation rates. However, as noted by these authors, this trend could be at least partially due to selection effects. Given the relatively small size of our sample and the large uncertainties (up to a factor of 10) inherent in UV continuum–derived SFRs (see Papovich et al. 2006), our results do not allow us to make strong statements about the SFRs of Lyα-emitting LBGs relative to the population as a whole.

5.3. *Correlation between* Lyα *Emission and Galaxy Size*

In Figure 10 we show z_{850}-band images (1.5″ thumbnails) for our entire spectroscopic sample (excluding UDF PFs i0). The

[12] We compute the errors on the fraction of LAEs assuming a binomial distribution. This assumes that systematic errors are small.

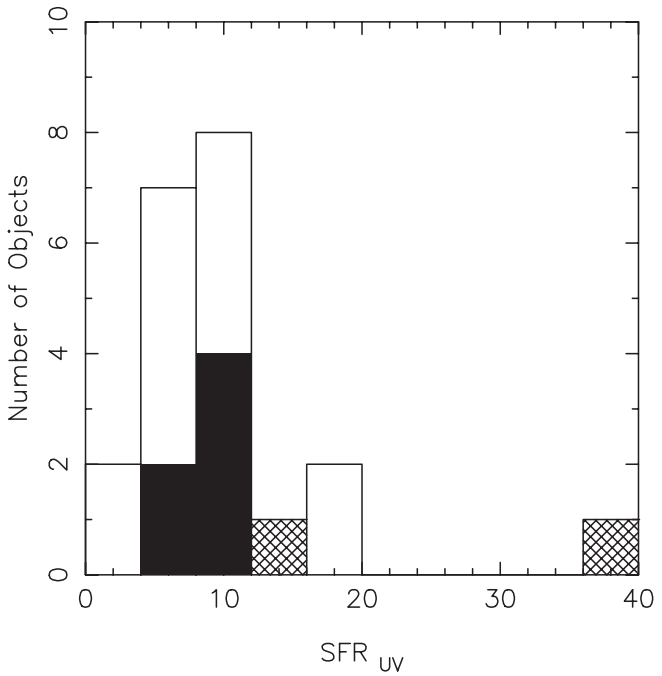

FIG. 9.—Histograms of SFR_{UV} for our spectroscopic sample. Sources in the Cl 1252 field were corrected for lensing by the cluster potential, except for objects BD 22 and BD 62, where the correction was highly uncertain. The filled histogram represents Lyα-emitting objects, and the cross-hatched histogram represents the confirmed $z \sim 6$ continuum objects lacking detectable Lyα emission. The Lyα-emitting objects appear to have values of SFR_{UV} very similar to that of the sample average (excluding the $6L_*$ galaxy BD 38).

uppermost six thumbnails are the confirmed Lyα-emitting LBGs, the two thumbnails in the bottom row are the confirmed $z \sim 6$ objects with no detectable Lyα emission, and the middle 13 are objects with no clear spectral features. The Lyα-emitting LBGs all have compact morphologies and show no morphological disturbances. However, the morphologies of BD 38 and BD 03 are very disturbed and extended, with "plumes" extending from a "core." Furthermore, the undetected objects overall have much more extended morphologies than the objects with detected Lyα emission.

Similarly, Stanway et al. (2004a, 2004b) confirmed that Lyα-emitting *i*-dropout objects have compact morphologies in the z_{850} band, with $0.09'' \leq r_{hl} \leq 0.14''$, where r_{hl} is the half-light radius. Moreover, SBM03#01 also appears compact in *HST* NICMOS 1.1 μm F110W-band and 1.6μm F160W-band imaging (Eyles et al. 2005). Interestingly, the Lyα-emitting $z = 5.78$ galaxy SBM03#03 discovered by Bunker et al. (2003) also has a very compact morphology ($r_{hl} \leq 0.08''$; marginally resolved in ACS imaging), despite being exceedingly bright ($z_{850} = 24.7$) for an *i*-dropout. This is in contrast to BD 38, a similarly bright ($z_{850} = 24.6$) *i*-dropout in our spectroscopic sample, but which is much more extended ($r_{hl} = 0.25''$) and lacks Lyα emission.

In the top panel of Figure 11, we plot the r_{hl} versus z_{850}-band magnitude for sources in our spectroscopic sample. The red circles show Lyα-emitting LBGs, the blue triangles represent BD 38 and BD 03 (sources with a continuum break), and the black squares show the *i*-dropouts in our sample without any clear spectral features. The Cl 1252 objects have been delensed. The 332 *i*-dropouts identified by Bouwens et al. (2006) over the two GOODS fields are shown with purple dots. Also included (*red asterisks*) are the four previously confirmed Lyα-emitting LBGs of Bunker et al. (2003) and Stanway et al. (2004a, 2004b) noted above, where the half-light radii and z_{850}-band magnitudes

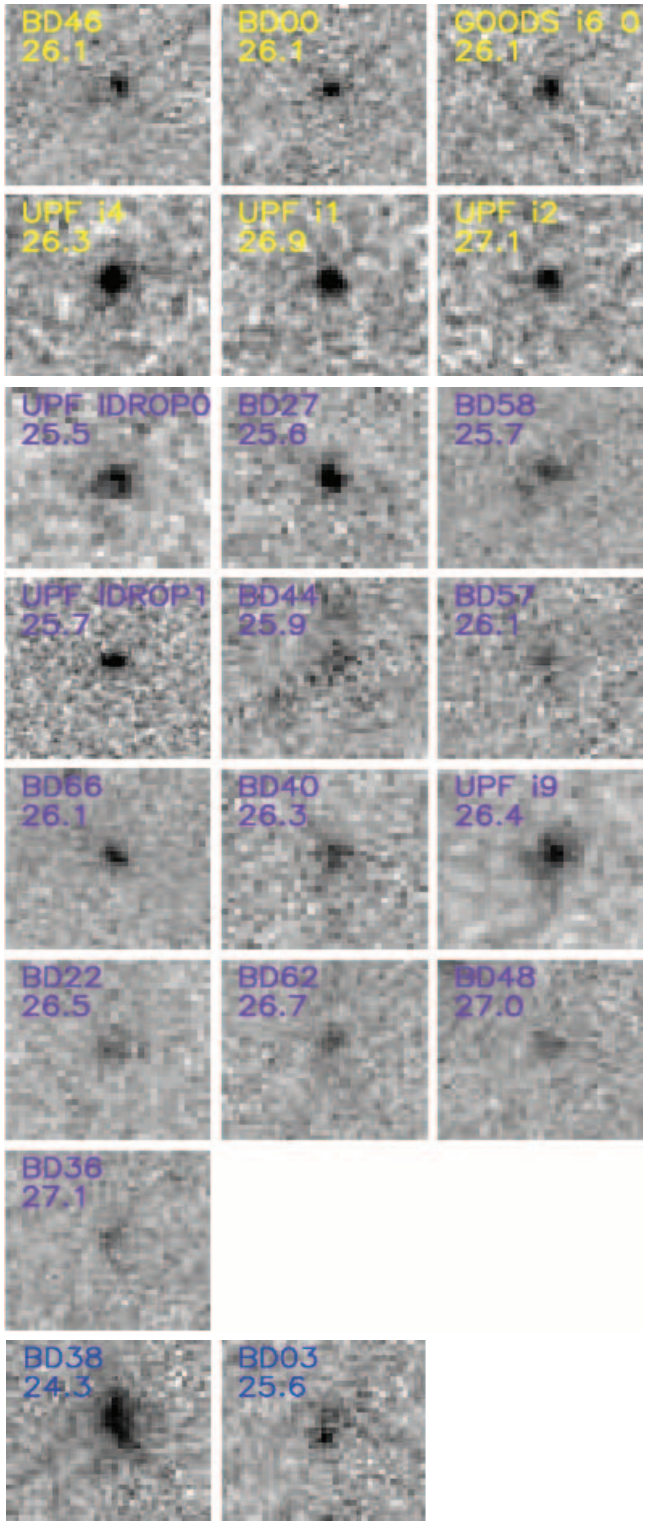

FIG. 10.—Thumbnail images of the entire spectroscopic sample in the z_{850} band (1.5″ on a side). Here "UDF PFs" is abbreviated as "UPF." The top six thumbnails show our Lyα-emitting sample, the bottom two show the confirmed $z \sim 6$ objects that are undetected in Lyα (BD 38 and BD 03), and the middle 13 show objects without any observed spectral features. The morphologies of BD 38 and BD 03 are much more disturbed than the Lyα-emitting LBGs. Furthermore, the majority of the undetected, fainter objects have a similar distorted morphology, in contrast to the very compact appearance of the Lyα-emitting LBGs.

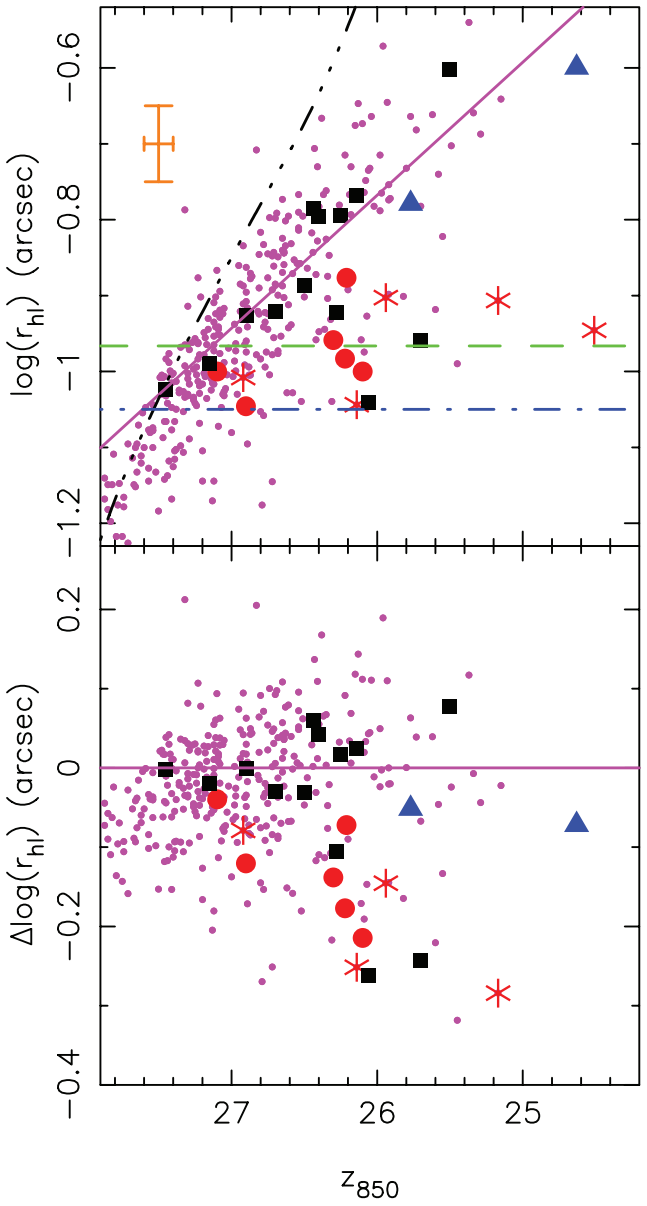

FIG. 11.—*Top*: Half-light radius vs. z_{850}-band magnitude. The small purple dots represent a sample of 332 *i*-dropouts selected over the GOODS fields (Bouwens et al. 2006). The red asterisks represent previously spectroscopically confirmed $z \sim 6$ Lyα-emitting LBGs (Bunker et al. 2003; Stanway et al. 2004a, 2004b; Vanzella et al. 2006). The other symbols are the same as in Fig. 6. The black triple-dot–dashed line shows the surface brightness selection limit of the Bouwens et al. (2006) sample. The purple line denotes the best linear fit to this sample (purple dots only; other objects excluded). The vertical orange error bar of $\sigma = 0.05$ dex indicates the scatter in the fit. The horizontal error bar indicates the typical photometric uncertainty. The blue dash-dotted line is the FWHM of the z_{850}-band PSF and represents a reasonable floor below which our size measurements become quite uncertain. *Bottom*: Residuals from the linear fit. The Bunker et al. (2003) object is outside the plot window ($\Delta \log r_{hl} = -0.49$). All Ly$\alpha$-emitting objects have half-light radii smaller than is typical for the 332 *i*-dropouts of Bouwens et al. (2006). A rank sum test performed on the objects from our spectroscopic sample supports the hypothesis (at $\geq$97% confidence) that Lyα-emitting *i*-dropouts (6 objects from our sample) are smaller than the objects without such emission (14 objects from our spectroscopic sample). Furthermore, the Lyα-emitting objects have a fairly constant size ($r_{hl} = 0.11'' \pm 0.01''$) over the entire range of luminosities probed.

quoted are taken from Bouwens et al. (2006).[13] The purple line in Figure 11 denotes a linear fit to the *i*-dropout sample (*purple dots*) of Bouwens et al. (2006). Objects with half-light radii smaller than the FWHM of the z_{850}-band point-spread function (PSF; 0.09″; *blue dash-dotted line*), fainter than our magnitude limit ($z_{850} > 27.8$), or brighter than $z_{850} = 25.0$ (due to a scarcity of bright sources) were not included in the fit. No sources from our spectroscopic sample were included in the fit.

We want to test the hypothesis that sources with Lyα emission are smaller on average than the *i*-dropout population in general. We chose not to use a χ^2 test, because it assumes a Gaussian scatter around the best-fit distribution. A better test is the rank sum test, using only the half-light radii of our spectroscopic sample. Using this test to compare our spectroscopic sample with the Bouwens et al. (2006) *i*-dropout sample, we find that the half-light radii of the galaxies in our spectroscopic sample are significantly (at $\geq$94% confidence) smaller than those of Bouwens et al. (2006). Restricting the rank sum test to include only objects in our spectroscopic sample also supports the hypothesis that Lyα-emitting *i*-dropouts are smaller than the rest of our sample at $\geq$97% confidence. Hence, Lyα-emitting *i*-dropouts seem to be morphologically distinct from other *i*-dropouts.

One potential exception to this rule is the object UDF 5225 of Rhoads et al. (2005), which has a "plume" of 1″ extending from a compact "core." This object was selected as a V_{606}-dropout, has a spectroscopic redshift of $z = 5.480$, and is too blue ($i_{775} - z_{850} \approx 0.5$) to be selected by *i*-dropout methods. However, even if we assumed that this object passed our color selection, the surface brightness of the plume is below our limiting surface brightness, due to shallower photometry than the UDF. Our deepest photometry (UDF PFs) of the object would only contain the brighter compact core. Hence, this object would not appear abnormal for Lyα-emitting objects in our sample.

Note that the nature of the vast majority of the objects (332 in total) used in our larger *i*-dropout sample is not known; however, from the discussion above, approximately 30% of these objects should be Lyα-emitting LBGs. If so, this would mitigate the differences observed between the sizes of Lyα-emitting LBGs and those from the *i*-dropout population in general (which include a significant fraction of Lyα-emitting sources). Hence, the size-luminosity discrepancy between Lyα-emitting and non-emitting LBGs would be larger than that quoted here.

This morphological difference may be due to the influence of the Lyα emission on the z_{850}-band flux. To date, the only confirmed $z \sim 6$ Lyα-emitting *i*-dropout with NICMOS imaging is SBM03#01 (Eyles et al. 2005), which, as noted above, is compact in both 1.1 μm F110W-band and 1.6 μm F160W-band imaging. Hence, the compact morphology of this LBG cannot simply be the result of its Lyα emission alone. NICMOS imaging of many more *i*-dropouts with confirmed Lyα emission is needed to determine the overall relevance of Lyα emission to the z_{850}-band morphology of these objects.

One potential physical explanation of this size deviation could lie in the masses of these objects. Lyα-emitting objects at $z \sim 3$–4 are found to have smaller stellar masses than objects lacking this emission (Overzier et al. 2006; Gawiser et al. 2006). This suggests that these objects may be associated with less massive dark matter halos. One would make a similar inference for the masses of these objects, using the observation that these objects are less dusty on average (Shapley et al. 2003; Gawiser et al. 2006), and thereby have fainter dust-corrected luminosities, than sources with no observable Lyα emission. Assuming that this translates to $z \sim 6$, and using the well-known correlation between size and mass (Mo et al. 1998), we would expect Lyα-emitting objects to appear smaller on average, which is what we observe.

We note that the recent results of Lai et al. (2007) on a sample of 12 $z \sim 5.7$ LAEs over the HDF-North GOODS area could be

[13] Object GOODS-N i'-drop 6 of Stanway et al. (2004a) is not included, due to its uncertain line identification.

seen to support this finding. Lai et al. (2007) found that 3 of the 12 sources were clearly detected in the IRAC data, and they inferred masses of 10^9–10^{10} $M_\odot$ through detailed stellar population modeling. While these masses are comparable to those of *i*-dropouts of similar luminosity studied over the GOODS fields (Yan et al. 2006; Eyles et al. 2007), the vast majority of LAEs in the Lai et al. (2007) sample (9 out of 12) are not detected in the GOODS IRAC imaging and hence will be significantly less massive than the 3 IRAC-detected LAEs. Although clearly a more careful comparison between these populations is needed, this suggests that $z \sim 5.7$ LAEs, on average, are somewhat less massive than the typical $z \sim 6$ star-forming galaxy.

5.4. *Preselecting Galaxies with* Lyα *Emission*

One interesting aspect of this morphology dependence on Lyα emission strength is in its potential to preselect Lyα-emitting *i*-dropouts for spectroscopic follow-up, similar to what is achieved in narrowband surveys. Confirmation rates of *i*-dropout–selected $z \sim 6$ LBGs are rather low ($\approx$30%), due to the low S/N of these objects in the continuum and the small fraction of LBGs with Lyα emission (§ 5.1). From our spectroscopic sample, we note that a simple size cut of $\Delta \log r_{\rm hl} \leq -0.05$ and magnitude cut of $z_{850} \geq 25.9$ would select five (83%) of the Lyα-emitting LBGs, while rejecting all but two (15%) of the sources without detectable Lyα emission. This would increase our success rate for spectroscopic confirmation by more than a factor of 3.

6. CONCLUSIONS

We have obtained spectroscopic observations of 22 *i*-dropouts drawn from two deep ACS fields. These dropouts were selected to have $i_{775} - z_{850}$ colors greater than 1.3. Spectroscopic redshifts for eight $z \sim 6$ objects in the RDCS 1252−2927 and Ultra Deep Field parallel fields were derived. We hereby confirm the effectiveness of the *i*-dropout technique of Bouwens et al. (2003, 2004a) in isolating a statistically relevant sample of $5.5 \leq z \leq 6.2$ star-forming galaxies.

No clear case of contamination by low-redshift sources was found in this sample. Together with the results of the complementary ACS grism survey of Malhotra et al. (2005), this suggests that our spectroscopic sample is dominated ($\geq$90%) by galaxies at $z \sim 6$. Six of the confirmed $z \sim 6$ objects possess measurable Lyα emission, with z_{850}-band magnitudes ranging from 26.1 to 27.1. The two brightest objects in our Cl 1252 sample are continuum sources that lack detectable Lyα emission, but show clear evidence for a Lyman break.

We compare our findings with other $z \sim 6$ *i*-dropout surveys, $z \approx 5.7$ narrowband surveys, and with the global properties of LBGs at $z \sim 3$ to determine the nature and composition of $z \sim 6$ galaxies. Our findings are as follows:

1. Significant ($W_{\rm Ly\alpha} \gtrsim 20$ Å) Lyα emission is detected in the spectra of only 30% of *i*-dropout objects. Using the model redshift distributions of Bouwens et al. (2006) to control for selection biases, we infer that only 32% ± 10% of star-forming galaxies at $z \sim 6$ show significant ($W_{\rm Ly\alpha} \gtrsim 20$ Å) Lyα emission (§ 5.1; Fig. 7), with an upper limit of 46% ± 11%. Moreover, the values of $W_{\rm Ly\alpha}$ of these objects on average are much smaller than those found for narrowband-selected LAEs. Since these trends are also evident in the LBG population at $z \sim 3$ (Shapley et al. 2003), this suggests that there is no strong change in the fraction of Lyα-emitting objects in the LBG population from $z > 5$ to $z < 4$.

2. The *i*-dropout technique misses $\approx$70% of the narrowband-selected $z \approx 5.7$ LAEs. Moreover, the LAEs that the *i*-dropout surveys do select show the weakest Lyα emission. This is a consequence of the Lyα emission in the i_{775}-band flux at $z \leq 5.9$. However, the selection efficiency increases strongly with redshift, due to Lyα emission shifting from the i_{775} to z_{850} bands. By $z \sim 6$, every z_{850}-band–detected Lyα emitter would be sampled by *i*-dropout techniques. Thus, over the whole redshift range sampled by the *i*-dropout technique, we expect to miss 10%–46% of the LAE population.

3. Lyα-emitting LBGs have similar z_{850}-band magnitudes and UV SFRs to those without detectable emission. However, no Lyα-emitting object in our sample has $z_{850} < 26.1$.

4. The size of Lyα-emitting objects is more compact than that predicted from the observed size-luminosity relation of 332 *i*-dropout galaxies. One possible explanation for this trend is that sources with Lyα emission may be systematically less massive than the typical *i*-dropout.

Most importantly, these results suggest that Lyα-emitting objects only constitute a modest fraction of the LBGs at $z \sim 6$ and thus do not provide us with a representative sample.

These results have important implications for how surveys for star-forming galaxies at $z \sim 6$ should be conducted. First, it appears that our spectroscopic success rates can be significantly enhanced by targeting *i*-dropouts with compact z_{850}-band morphologies. From our sample, we find that the criteria $z_{850} \geq 25.9$ and $\Delta \log r_{\rm hl} \leq -0.05$ select $\geq$80% of Lyα-emitting objects, while rejecting $\geq$80% of the remaining sample.

Second, it appears that wide-area narrowband surveys miss $\approx$70% of the broadband-selected LBG population at $z \sim 6$, and, as seen in Figure 11, the objects that they do find are intrinsically different from the *i*-dropout LBG population as a whole. On the other hand, broadband surveys miss the strongest Lyα emitters at $5.5 \leq z \leq 5.8$ that narrowband surveys sample. Therefore, it appears that a combination of surveys, taking advantage of the strengths of both narrowband and broadband selection techniques, will be necessary to obtain a complete characterization of the star-forming population at $z \sim 6$.

We would like to thank Dan Kelson for useful discussions concerning spectral reduction and David Koo for his helpful insights. ACS was developed under NASA contract NAS5-32864, and this research was supported by NASA grant NAG5-7697. The authors wish to recognize and acknowledge the very significant cultural role and reverence that the summit of Mauna Kea has always had within the indigenous Hawaiian community. We are most fortunate to have the opportunity to conduct observations from this mountain.

REFERENCES

Ajiki, M., Mobasher, B., Taniguchi, Y., Shioya, Y., Nagao, T., Murayama, T., & Sasaki, S. S. 2006, ApJ, 638, 596
Ajiki, M., et al. 2003, AJ, 126, 2091
Ando, M., Ohta, K., Iwata, I., Watanabe, C., Tamura, N., Akiyama, M., & Aoki, K. 2004, ApJ, 610, 635
Bennett, C. L., et al. 2003, ApJS, 148, 97
Bertin, E., & Arnouts, S. 1996, A&AS, 117, 393
Bouwens, R. J., & Illingworth, G. D. 2006, Nature, 443, 189
Bouwens, R. J., Illingworth, G. D., Blakeslee, J. P., & Franx, M. 2006, ApJ, 653, 53
Bouwens, R. J., et al. 2003, ApJ, 595, 589
———. 2004a, ApJ, 606, L25
———. 2004b, ApJ, 616, L79
Brocklehurst, M. 1971, MNRAS, 153, 471

Bunker, A. J., Stanway, E. R., Ellis, R. S., McMahon, R. G., & McCarthy, P. J. 2003, MNRAS, 342, L47
Dawson, S., et al. 2004, ApJ, 617, 707
Dey, A., Spinrad, H., Stern, D., Graham, J. R., & Chaffee, F. H. 1998, ApJ, 498, L93
Dickinson, M. 1999, in AIP Conf. Proc. 470, After the Dark Ages: When Galaxies Were Young (the Universe at $2 < z < 5$), ed. S. Holt & E. Smith (New York: AIP), 122
Dickinson, M., et al. 2004, ApJ, 600, L99
Dow-Hygelund, C. C., et al. 2005, ApJ, 630, L137
Eyles, L. P., Bunker, A. J., Ellis, R. S., Lacy, M., Stanway, E. R., Stark, D. P., & Chiu, K. 2007, MNRAS, 374, 910
Eyles, L. P., Bunker, A. J., Stanway, E. R., Lacy, M., Ellis, R. S., & Doherty, M. 2005, MNRAS, 364, 443
Fan, X., et al. 2001, AJ, 122, 2833
———. 2003, AJ, 125, 1649
Gawiser, E., et al. 2006, ApJ, 642, L13
Giacconi, R., et al. 2002, ApJS, 139, 369
Giavalisco, M., et al. 2004, ApJ, 600, L103
Hall, P. B., Martini, P., Depoy, D. L., & Gatley, I. 1997, ApJ, 484, L17
Hopkins, A. M. 2004, ApJ, 615, 209
Hu, E. M., Cowie, L. L., Capak, P., McMahon, R. G., Hayashino, T., & Komiyama, Y. 2004, AJ, 127, 563 (Hu04)
Hu, E. M., Cowie, L. L., McMahon, R. G., Capak, P., Iwamuro, F., Kneib, J.-P., Maihara, T., & Motohara, K. 2002, ApJ, 568, L75
Iye, M., et al. 2006, Nature, 443, 186
Kashikawa, N., et al. 2006, ApJ, 648, 7
Kelson, D. D. 2003, PASP, 115, 688
Kennicutt, R. C., Jr. 1998, ARA&A, 36, 189
Kneib, J., Ellis, R. S., Santos, M. R., & Richard, J. 2004, ApJ, 607, 697
Kodaira, K., et al. 2003, PASJ, 55, L17
Kurk, J. D., Cimatti, A., di Serego Alighieri, S., Vernet, J., Daddi, E., Ferrara, A., & Ciardi, B. 2004, A&A, 422, L13
Lai, K., Huang, J.-S., Fazio, G., Cowie, L. L., Hu, E. M., & Kakazu, Y. 2007, ApJ, 655, 704
Lehnert, M. D., & Bremer, M. 2003, ApJ, 593, 630
Lidman, C., Rosati, P., Demarco, R., Nonino, M., Mainieri, V., Stanford, S. A., & Toft, S. 2004, A&A, 416, 829
Loeb, A., & Barkana, R. 2001, ARA&A, 39, 19
Lombardi, M., et al. 2005, ApJ, 623, 42
Madau, P. 1995, ApJ, 441, 18
Madau, P., Pozzetti, L., & Dickinson, M. 1998, ApJ, 498, 106
———. 2004, ApJ, 617, L5
Malhotra, S., et al. 2005, ApJ, 626, 666
Massey, P., & Gronwall, C. 1990, ApJ, 358, 344
Massey, P., Strobel, K., Barnes, J. V., & Anderson, E. 1988, ApJ, 328, 315
Mo, H. J., Mao, S., & White, S. D. M. 1998, MNRAS, 295, 319
Nagao, T., et al. 2004, ApJ, 613, L9
Oke, J. B., & Gunn, J. E. 1983, ApJ, 266, 713
Oke, J. B., et al. 1995, PASP, 107, 375
Osterbrock, D. E. 1989, Astrophysics of Gaseous Nebulae and Active Galactic Nuclei (Mill Valley: University Science Books)
Overzier, R., et al. 2006, ApJ, submitted
Papovich, C., et al. 2006, ApJ, 640, 92
Rhoads, J. E., & Malhotra, S. 2001, ApJ, 563, L5
Rhoads, J. E., et al. 2003, AJ, 125, 1006
———. 2004, ApJ, 611, 59
———. 2005, ApJ, 621, 582
Rosati, P., della Ceca, R., Norman, C., & Giacconi, R. 1998, ApJ, 492, L21
Rosati, P., et al. 2004, AJ, 127, 230
Salpeter, E. E. 1955, ApJ, 121, 161
Shapley, A. E., Steidel, C. C., Pettini, M., & Adelberger, K. L. 2003, ApJ, 588, 65
Shimasaku, K., Ouchi, M., Furusawa, H., Yoshida, M., Kashikawa, N., & Okamura, S. 2005, PASJ, 57, 447
Shimasaku, K., et al. 2006, PASJ, 58, 313
Songaila, A. 2004, AJ, 127, 2598
Spinrad, H., Dey, A., Stern, D., Dunlop, J., Peacock, J., Jimenez, R., & Windhorst, R. 1997, ApJ, 484, 581
Spinrad, H., Stern, D., Bunker, A., Dey, A., Lanzetta, K., Yahil, A., Pascarelle, S., & Fernández-Soto, A. 1998, AJ, 116, 2617
Stanway, E., McMahon, R., & Bunker, A. 2005, MNRAS, 359, 1184
Stanway, E. R., Bunker, A. J., & McMahon, R. G. 2003, MNRAS, 342, 439
Stanway, E. R., Bunker, A. J., McMahon, R. G., Ellis, R. S., Treu, T., & McCarthy, P. J. 2004a, ApJ, 607, 704
Stanway, E. R., et al. 2004b, ApJ, 604, L13
Steidel, C. C., Adelberger, K. L., Giavalisco, M., Dickinson, M., & Pettini, M. 1999, ApJ, 519, 1
Steidel, C. C., Pettini, M., & Hamilton, D. 1995, AJ, 110, 2519
Stern, D., Bunker, A., Spinrad, H., & Dey, A. 2000, ApJ, 537, 73
Stern, D., & Spinrad, H. 1999, PASP, 111, 1475
Stern, D., Yost, S. A., Eckart, M. E., Harrison, F. A., Helfand, D. J., Djorgovski, S. G., Malhotra, S., & Rhoads, J. E. 2005, ApJ, 619, 12
Taniguchi, Y., Shioya, Y., Ajiki, M., Fujita, S. S., Nagao, T., & Murayama, T. 2003, J. Korean Astron. Soc., 36, 123
Taniguchi, Y., et al. 2005, PASJ, 57, 165
van der Wel, A., Franx, M., van Dokkum, P., Rix, H.-W., Illingworth, G., & Rosati, P. 2005, ApJ, 631, 145
Vanzella, E., et al. 2005, A&A, 434, 53
———. 2006, A&A, 454, 423
Weymann, R. J., Stern, D., Bunker, A., Spinrad, H., Chaffee, F. H., Thompson, R. I., & Storrie-Lombardi, L. J. 1998, ApJ, 505, L95
Yan, H., Dickinson, M., Giavalisco, M., Stern, D., Eisenhardt, P. R. M., & Ferguson, H. C. 2006, ApJ, 651, 24